

REVIEW OF WAVE-DRIVEN SEDIMENT RESUSPENSION AND TRANSPORT IN ESTUARIES

Malcolm O. Green¹ and Giovanni Coco²

Received 30 June 2013; revised 28 November 2013; accepted 3 December 2013.

[1] Waves are fundamentally important to the physical and biological functioning of estuaries. Understanding and predicting contaminant transport, development of sedimentary structures, geomorphological response to changes in external forcings such as rising sea level, and response of estuarine ecosystems to contaminant stressors require understanding of the relative roles of wave- and current-driven sediment transport. We review wave-driven sediment resuspension and transport in estuaries, including generation of bed shear stress by waves, initiation of sediment motion by waves, and the ways waves modulate, add to, and interact with sediment transport driven by currents. A key characteristic of the wave-induced force on the seabed is extreme spatial and temporal variations; simple analytical models are revealing of the way such patterns develop. Statistical methods have

been widely applied to predict wave resuspension of intertidal-flat bed sediments, and physically based predictors of resuspension developed from open-coast studies appear to also apply to short-period estuarine waves. There is ample experimental evidence to conclude that over the long term, waves erode and tidal currents accrete intertidal flats. Waves indirectly add to the formation of fluid mud by adding to the estuarine pool of fine sediment, and waves may fluidize subtidal seabeds, changing bed erodibility. Models have been used to explore the dynamic balance between sediment transport by waves and by currents and have revealed the key control of waves on estuarine morphology. Estuarine intertidal flats are excellent natural laboratories that offer opportunities for working on a number of fundamental problems in sediment transport.

Citation: Green, M. O., and G. Coco (2014), Review of wave-driven sediment resuspension and transport in estuaries, *Rev. Geophys.*, 52, doi:10.1002/2013RG000437.

1. INTRODUCTION

[2] Waves play a fundamental role in the physical and biological functioning of estuarine systems. With respect to **sediment transport**, the focus of this review, waves and currents are the primary mechanisms of sediment **resuspension** in estuaries. Waves are **locally generated** by the wind acting on the **fetch** inside the estuary basin, and they may also propagate into the basin from the ocean; currents are tidal, wind driven and density driven. Whereas periods of locally generated waves are 0.5–5 s and ocean-wave periods may exceed 20 s, currents vary on timescales of tens of minutes to hours [Shi *et al.*, 2006].

[3] Unlike tidal currents, which are periodic, waves occur episodically. Because waves generated inside estuarine basins

by winds have a typically short period, **wave-orbital motions** are more likely to be able to penetrate down to the bed and resuspend sediments only on intertidal flats and only then toward low tide. Nevertheless, orbital motions under even very small waves—less than 20 cm high—have been shown to be capable of resuspending intertidal-flat sediments [e.g., Anderson, 1972; Dyer *et al.*, 2000; Uncles and Stephens, 2010; Green, 2011]. Wave resuspension tends to switch off at some point in a rising tide and switch back on again in the falling tide as the part of the water column in which wave-orbital motions are strong enough to resuspend sediments is raised and lowered by the tide. Nevertheless, episodic sediment resuspension by waves adds to and even masks periodic resuspension by currents. For example, Sanford [1994] found that wave-forced resuspension exceeded tidal resuspension by a factor of 3–5 on a mud bed in the Upper Chesapeake Bay; Christie *et al.* [1999] reported an order-of-magnitude increase in **suspended-sediment concentration** during storms (causing the system to become wave dominated) compared to during fair weather (tide dominated) on an intertidal flat in the **macrotidal** Humber estuary (UK); and Ralston and Stacey [2007] described how suspended-sediment concentration on

¹National Institute of Water and Atmospheric Research, Hamilton, New Zealand.

²Instituto de Hidráulica Ambiental IH Cantabria, University of Cantabria, Santander, Spain.

Corresponding author: M. O. Green, National Institute of Water and Atmospheric Research, PO Box 11-115, Hamilton, Waikato 3216, New Zealand. (m.green@niwa.co.nz)

a **microtidal** intertidal flat in San Francisco Bay (USA) drops rapidly as winds and waves abate. *Green et al.* [1997] described a **mesotidal** intertidal flat (Manukau Harbour, New Zealand) where tidal currents were incapable of resuspending sediments and resuspension was completely controlled by (episodically occurring) waves.

[4] Particulate matter resuspended by locally generated **wind waves** may have adverse ecological effects on bivalve condition [*Ellis et al.*, 2002], light climate [*Lawson et al.*, 2007; *Verspecht and Pattiaratchi*, 2010], and sea grass health and distribution [*Lewis et al.*, 1985; *Turner et al.*, 1999; *Moore and Wetzel*, 2000]. However, wave resuspension has also been shown to cleanse bed sediments of heavy metals [*Williamson et al.*, 1996], to hasten the recovery of benthic macrofauna from smothering by sediment deposition [*Norkko et al.*, 2002], to nourish vegetated habitats with sediment [*Carling*, 1982], and to play a central role in estuarine phytoplankton trophic dynamics [e.g., *Demers et al.*, 1987; *de Jonge and van Beusekom*, 1992].

[5] From a geomorphological point of view, waves drive seasonal variations in sedimentation [*de Haas and Eisma*, 1993], control direction (onshore or offshore) of fine-sediment transport on intertidal flats [*Christie et al.*, 1999], build small-scale ripple and large-scale **ridge-and-runnel** topographies [*Dolphin et al.*, 1995; *Christiansen et al.*, 2006], and interact with tidal currents to maintain intertidal flats in a type of dynamic equilibrium [e.g., *Roberts et al.*, 2000]. Waves have been shown to explain the distribution of intertidal flats and salt marsh in microtidal estuaries *Fagherazzi et al.* [2007] and to control the long-term evolution of marsh boundaries [*Marani et al.*, 2011; *Mariotti and Fagherazzi*, 2013a; *Francalanci et al.*, 2013], and waves have been invoked to explain large-scale patterns of surficial-sediment texture [*Ryan and Cooper*, 1998; *Malvarez et al.*, 2001].

[6] Our aim is to review wave-driven sediment transport in estuaries, which includes the generation of **bed shear stress** by waves, the initiation of sediment motion by waves, and the ways waves modulate, add to, and interact with sediment transport driven by currents in estuaries.

[7] We focus on the interior of the estuary, which includes unvegetated intertidal flats, as opposed to marginal habitats, which include mangroves and salt marshes. We refer the reader to reviews of tidal salt marsh morphodynamics by *Friedrichs and Perry* [2001] and *Townend et al.* [2011] and note that there is a large body of literature that shows that where microtidal intertidal flats are backed by tidal marshes, large waves combined with wind-driven **storm surges** sustain the marshes by nourishing them with sediment. This is promoted by the combination of a large wave-driven suspended-sediment load, increased duration of inundation under the storm surge, and the baffling effect of vegetation. Where marshes are at the head of a steep intertidal flat, storm waves may attack the marsh edge directly, causing erosion. The reader is referred to *Fagherazzi et al.* [2012], who review numerical models of salt marsh evolution, which includes treatment of marsh-edge erosion by waves. We also do not consider open-coast intertidal flats; there is a large literature

on southeast Asian open-coast flats that is accessible through, for instance, *Yang et al.* [2003] and *Wang et al.* [2002], who review muddy tidal flats on the open coast of China. We do not discuss estuarine beaches; the reader is referred to *Jackson et al.* [2002] and to *Nordstrom and Jackson* [2012] for reviews of beaches in short-fetch environments, which include estuaries.

[8] Section 2 reviews the generation and dissipation of estuarine wind waves, as background to understanding the wave-induced bed shear stress. Particular attention is given to spatial (across intertidal flats) and temporal (over tidal cycles) patterns in stress under locally generated wind waves. We comment on the influence of ocean waves that may penetrate the interior of an estuary from time to time and on wave-current interaction.

[9] Section 3 reviews the wave resuspension of bed sediments. We show data that confirm that waves, when present, can dominate resuspension on intertidal flats and that spatial and temporal patterns of suspended sediment follow spatial and temporal patterns of wave-induced bed shear stress.

[10] Section 4 reviews the ways waves modulate, add to, and interact with sediment transport driven by currents. We distinguish between the direct transport of suspended sediment by waves and the transport by tidal currents of sediments that are resuspended from the bed by waves. We also look at wave fluidization of muddy beds, which can initiate various forms of mud transport.

[11] Section 5 provides a brief look at exploratory models that investigate and explain the dynamic balance amongst sediment transport by waves, sediment transport by currents, and intertidal-flat morphology. “Exploratory model” is meant in the sense of *Murray* [2003], being a model that has as few processes as possible, aims to represent the remaining processes as simply as possible, and is built with the aim of developing an understanding of why a system behaves as it does. For a detailed review of morphodynamic modeling of intertidal flats, the reader is referred to *de Swart and Zimmerman* [2009] and *Friedrichs* [2011].

[12] Section 6 provides some recommendations for future research.

2. WAVE-GENERATED BED SHEAR STRESS

[13] Under typical-period estuarine wind waves (1–5 s), the ratio of wind-wave wavelength to water depth varies significantly over the tidal cycle, which causes a corresponding variation in **wave-orbital speed** at the bed and associated wave-induced bed shear stress. Even in quite shallow water, orbital motions under estuarine waves may not penetrate down from the sea surface to the seabed; for instance, a 1.5 s period wave with a wavelength of 3.5 m is a deepwater wave in water depths greater than just 1.75 m, and the wave-orbital speed at the bed in that case will be virtually zero. Water depth, therefore, is a key control on the wave-induced bed shear stress, and waves accordingly are more effective at resuspension on intertidal flats than in channels, because the former are shallower.

[14] Under pure waves (i.e., with no superimposed current), the wave-induced bed shear stress τ_w is typically conceived of as a **quadratic bottom friction**:

$$\tau_w = \frac{1}{2}\rho f_w U_{w,b}^2 \quad (1)$$

where ρ is water density, f_w is the **wave friction factor**, and $U_{w,b}$ is the maximum over-the-wave-cycle horizontal wave-orbital speed at the bed. When the wave **boundary layer** is hydraulically rough turbulent, the wave friction factor, by definition [see *Nielsen*, 1992], depends solely on the **bed roughness** k_b relative to the **wave-orbital semiexcursion** at the bed A_b . For example, *Swart* [1974] proposed

$$f_w = \exp\left[5.213(k_b/A_b)^{0.194} - 5.977\right] \quad (2)$$

where $A_b = U_{w,b}T/2\pi$ or

$$f_w = 1.39(A_b/k_b)^{-0.52} \quad (3)$$

where $A_b = U_{w,b}T$ [*Soulsby*, 1997] and T is the wave period, which should also be evaluated at the bed. Following the scaling arguments of, for example, *Smith and McLean* [1977], k_b may be evaluated as a **grain roughness** in which case the wave friction factor becomes a skin-friction wave friction factor and τ_w becomes a **skin friction**, which is the component of the bed shear stress that is thought to act on the bed-sediment grains, causing resuspension when the critical bed shear stress for initiation of sediment motion is exceeded. In the case of equation (2), the grain roughness is given as $2.5D_{50}/30$ and for equation (3) it is given as $2\pi D_{50}/12$, where D_{50} is the median grainsize of the bed sediment.

2.1. Locally Generated Wave Field

[15] From the point of view of the wave-induced bed shear stress, the two important wave parameters are the wave height H and the wave period T , since these govern the wave-orbital speed at the bed at any given water depth h . For linear waves, this is expressed as

$$U_{w,b} = \frac{\pi H}{T \sinh(kh)} \quad (4)$$

where T is related to wavelength L by the linear wave dispersion relationship $\omega^2 = gk \tanh(kh)$, $\omega = 2\pi/T$ is the wave radian frequency, $k = 2\pi/L$ is the wave number, and g is acceleration due to gravity. Height and period of locally generated wind waves depend on fetch length, wind speed, duration over which the wind blows, and water depth. However, *le Hir et al.* [2000] pointed out that duration is frequently not a limiting factor in estuaries since, for typical estuarine fetch lengths of order 1 km, waves reach their fully developed state over a small fraction of the tidal cycle.

[16] *Fagherazzi and Wiberg* [2009] noted that for short fetches, the height of waves in shallow water is similar to that of waves in deep water (for the same wind speed), but as the fetch increases, wave growth is reduced compared to that in deep water and the wave frequency is higher. *Fagherazzi and Wiberg* noted that to their knowledge, “a wave model explicitly developed from extensive wave datasets in shallow

coastal bays is still unavailable”, and chose as the best option for now the formulation of *Young and Verhagen* [1996a, 1996b], which they gave as

$$\epsilon = 0.00364 \left\{ \tanh A_1 \tanh \left(\frac{B_1}{\tanh A_1} \right) \right\}^{1.74} \quad (5)$$

where

$$A_1 = 0.493\delta^{0.75} \quad (6)$$

$$B_1 = 0.00313\chi^{0.57} \quad (7)$$

and

$$\zeta = 0.133 \left\{ \tanh A_2 \tanh \left(\frac{B_2}{\tanh A_2} \right) \right\}^{-0.37} \quad (8)$$

where

$$A_2 = 0.331\delta^{1.01} \quad (9)$$

$$B_2 = 5.215 \times 10^{-4} \chi^{0.73} \quad (10)$$

[17] Here $\epsilon = g^2 E / U_{\text{wind}}^4$ is the **dimensionless** wave energy ($E = \rho g H_s^2 / 16$ is the wave energy, where H_s is the **significant wave height**), $\zeta = f U_{\text{wind}} / g$ is the dimensionless **spectral-peak wave frequency** (f is spectral-peak wave frequency), $\chi = gF / U_{\text{wind}}^2$ is the dimensionless fetch (F is fetch), $\delta = gh / U_{\text{wind}}^2$ is the dimensionless water depth, and U_{wind} is the reference wind speed at an elevation of 10 m. *Young and Verhagen*'s formulation is based on full-scale experimental data in water depths similar to shallow coastal lagoons and has been tested with favorable results in the shallow, microtidal Venice Lagoon (Italy) by *Carniello et al.* [2011]. *Fagherazzi and Wiberg* noted that recent advanced numerical wave models use this same type of analytical formulation of the relationship between wave parameters and fetch, depth, and wind speed.

[18] *Etemad-Shahidi et al.* [2009] compared three other simplified methods and tested their performance using data from Lake Ontario and Lake Erie (North America). All methods performed well, particularly under fetch-limited conditions, although they all slightly underestimated wave height. The use of simplified methods greatly reduces the computational cost of numerical simulations and has recently been implemented in studies of long-term morphological change [e.g., *Tambroni and Seminara*, 2012; *Spearman*, 2011].

[19] The spectral formulation of the **wave-action conservation equation** originally derived by *Hasselmann et al.* [1973], and as written by *Carniello et al.* [2005], provides an alternative wave predictor:

$$\frac{\partial N}{\partial t} + \frac{\partial(c_{gx}N)}{\partial x} + \frac{\partial(c_{gy}N)}{\partial y} + \frac{\partial(c_{\omega}N)}{\partial \omega} + \frac{\partial(c_{\theta}N)}{\partial \theta} = \frac{S}{\omega} \quad (11)$$

where t is time, x and y are horizontal coordinates, θ is direction of wave propagation, $c = \omega/k$ is the wave phase speed, c_{gx} and c_{gy} are the x and y components of the wave group speed c_g , and N is the wave action, which is equal to the ratio of wave energy and the wave frequency ω . The S represents sources (wave growth) and sinks (wave decay) related to

wind energy transfers, nonlinear wave interactions, frictional dissipation, **whitecapping**, and **depth-limited breaking**.

[20] A widely used solver of the wave-action equation is the spectral model SWAN [Booij *et al.*, 1999], which has been successfully applied in a variety of environments including shallow estuaries [e.g., Umgiesser *et al.*, 2004; Chen *et al.*, 2005; Lettmann *et al.*, 2009]. Other solvers primarily differ in the numerical scheme or in the formulations describing sources and sinks [e.g., Ferrarin *et al.*, 2008]. Simplified versions of the wave-action equation assume a constant ω in space and time (which implies that the fourth term in the wave-action equation goes to zero) and an instantaneous adjustment between wind and wave direction (which implies that the fifth term in the wave-action equation goes to zero). Solution of the resulting equation is less complicated than the original case but still provides good agreement with observations [Carniello *et al.*, 2005].

[21] Mariotti and Fagherazzi [2013b] compared wave **events** measured at several locations on a mesotidal mudflat in Willapa Bay (Washington, USA) to hindcasts by Young and Verhagen's [1996a, 1996b] equations (hereinafter Y&V) and the SWAN model. The SWAN model was applied in both a 1-D and a 2-D geometry: the 2-D case covered the southern portion of Willapa Bay (6×10 km) and the 1-D case treated a flat **bathymetry**. To account for the fact that fetch depends strongly on wind direction at the Willapa Bay site, a single value of fetch was determined for each wind direction. During each event, water depth was modulated by the tide (0 to 3.5 m; mean depth 1.5 m), and wind speed ranged between 5 and 20 m/s (mean 10 m/s). Both H_s and the spectral-peak wave period showed a strong dependence on water depth and wind speed, with both being larger in greater water depths and under greater wind speeds. Two different formulations for the bed friction were tested, and lower friction coefficients were found to produce a smaller error in wave height but a larger error in wave period. Comparison of model hindcasts with measurements showed that the 2-D and 1-D SWAN models reproduced wave height equally well and better than the Y&V equations under the different conditions of wind speed, water level, and fetch. Y&V tended to underpredict wave heights for all water depths and wind speeds. In contrast, wave periods were reproduced equally well by SWAN and Y&V.

[22] Figure 10 of Carniello *et al.* [2005] is a good example of an estuarine wind-wave field that displays spatial and temporal variability that is typical of shallow estuaries. The data were simulated by a coupled wind wave-tide model and represent waves generated by a steady wind at a low tide and at a high tide. The simulation is for the Venice Lagoon, which is shallow and complex, with islands and intertidal flats and an intricate channel network. The wave model simulated wind-wave generation and propagation by solving a simplified form of the wave-action equation that included positive and negative source terms, and the tide model solved the two-dimensional **shallow-water equations** while accounting for wetting and drying in intertidal areas. At each time step, the tide model provided water levels to the wave model, which was used to predict wave propagation and

energy losses by bottom friction and depth-limited breaking. This coupling with the tide model was viewed as being crucial to correctly predict the wave field. Carniello *et al.* noted the significant influence of the tide on the wave field, with wave height following the tidal change in water level, such that waves were highest and longest around the time of high tide, when the fetch was greatest and wave interaction with the bottom was least. Spatial variation of wave height was caused by downwind fetch extension, by interruption of the fetch by tidally emergent sandbanks and islands, and by depth-dependent dissipation and wave breaking. This is a common feature of the wave field in estuaries with a large intertidal area relative to subtidal area [Smith *et al.*, 2001].

2.2. Dissipative Processes

[23] Especially on intertidal flats, energy losses are important. Energy losses are incurred by dissipation at the seabed (which may be caused by friction, **percolation**, scattering, and coupling of the wave motion with a **viscoelastic** mud bed), **steepness-limited wave breaking**, and depth-induced breaking. le Hir *et al.* [2000] demonstrated the importance of dissipation of wave energy by bottom friction in an analysis that was motivated by measurements from the macrotidal Brouage mudflat (France) that showed a linear relationship between maximum wave height and local water depth. The significant wave height did not exceed 0.15 times the depth, which is well below the commonly adopted limit of $0.7 h$. Similar observations had been reported by Wells and Kemp [1986] from the Surinam coast, and the discrepancy between the observations and the usual limit was explained in that case by energy dissipation arising from coupling of the wave motion with a viscoelastic mud bed. le Hir *et al.* pursued an alternative explanation for the Brouage data, given that **liquefaction** of the bed is not known to occur at Brouage. Using **linear wave theory** and applying the conservation of energy for a **monochromatic** wave propagating on a profile with uniform slope, le Hir *et al.* showed that **wave attenuation** by quadratic bottom friction depends on the dimensionless parameter f_w/β , where β is the slope of the bottom profile. For small values of f_w/β , dissipation is negligible and wave height is maintained or even increased (by **shoaling**) until the wave breaks; for large f_w/β , dissipation dominates and the waves come to be saturated, meaning that wave height tends to a constant limiting proportion of the water depth, $(H/h)_{\text{lim}}$, which is given by

$$\left(\frac{H}{h}\right)_{\text{lim}} = \frac{15\pi}{4} \frac{\beta}{f_w} \quad (12)$$

where the constant is likely to vary depending on the exact definition of wave height used. Equation (12) gives the maximum wave height that a tidal flat can experience at a given water depth. Using equation (12), le Hir *et al.* deduced $f_w = 0.05$ from the Brouage data, which is physically reasonable and indicative that **wave dissipation** by bottom friction can provide a complete explanation for the wave observations. Kim [2003] applied shallow-water wave theory to find an analytical solution to the differential equation developed by

le Hir *et al.* [2000] to obtain the following equation for wave-height attenuation across the profile with uniform slope:

$$\frac{H}{h_0} = \left[\frac{4 f_w}{15\pi \beta} X^{-1} + \left(\frac{h_0}{H_0} - \frac{4 f_w}{15\pi \beta} \right) X^{1/4} \right]^{-1} \quad (13)$$

[24] Here H_0 is the wave height at the outer end of the profile where the water depth is h_0 , $X=x\beta/h_0$ is the normalized distance offshore (which is equivalent to the normalized water depth h/h_0 on a profile with uniform slope), and x is the distance offshore (positive) where $x=0$ at the landward end of the profile. Equation (13) is likely to underestimate wave height along the seaward part of the profile where the shallow-water equations overestimate $U_{w,b}$, which therefore overestimates dissipation. *Green and Coco* [2007] presented wave-height data from a microtidal intertidal flat (Waikopua, New Zealand) that were at least partially consistent with equation (13) with $f_w=0.015$, which in turn was estimated from the measured bed-sediment grainsize, wave period, and wave-orbital speed at the bed. Pressure measured at the seabed was used to estimate wave height. However, the pressure signal under waves is increasingly attenuated with increasing distance below the mean water level, which reduces the information about the surface waves in the pressure signal; this necessitated the truncation of the analysis around high tide. Also, the analysis neglected any possible cross-flat change in the wave friction factor due to the presence of mangrove pneumatophores (breathing roots that grow upward out of the water) at intertidal-flat elevations greater than about mean sea level. An increase in surface friction resulting from the presence of vegetation strongly affects wave attenuation and causes, for salt marshes, a reduction in wave height that scales exponentially with the width of the vegetated area [Brampton, 1992; Moller *et al.*, 1999].

2.3. Wave-Orbital Speed at the Bed

[25] Changes in $U_{w,b}$ are driven by changes in the intrinsic properties of the waves (height and period) and by changes in the ratio of wavelength to water depth. For instance, *Green et al.* [1997] noted that $U_{w,b}$ attained a maximum around midtide on both **flooding** and **ebbing** tides. When the water was deeper than it was at midtide, the waves were larger as a consequence of the larger fetch, but the greater depth attenuation of the orbital motions reduced $U_{w,b}$ relative to $U_{w,b}$ at midtide. When the water was shallower than it was at midtide, depth attenuation was less but the wave height was smaller under the reduced fetch, thus causing $U_{w,b}$ to be smaller than it was at midtide. Other researchers have confirmed this pattern. For instance, *Christie et al.* [1999] showed maximum current speeds under waves occurring around midtide and minimum currents at high tide.

2.4. Bed Shear Stress

[26] Since τ_w scales with the square of $U_{w,b}$ (equation (1)) and $U_{w,b}$ at any location varies significantly with tidal changes in water depth (section 2.3), we can expect tidal-cycle variation in wave-induced bed shear stress to be pronounced. Understanding that there is an intrinsic connection between temporal and

spatial variations, we can deduce the tidal-cycle variation in τ_w by looking first at the cross-flat variation in τ_w , which we do in the following.

2.4.1. Spatial Patterns in Bed Shear Stress

[27] The formulation by *le Hir et al.* [2000] of wave attenuation by frictional dissipation provides an excellent platform for exploring the basic controls on the cross-flat variation in τ_w . Inserting into equation (1) the linear shallow-water approximation for $U_{w,b}$, given by

$$U_{w,b} = (H/2)\sqrt{g/h} \quad (14)$$

yields an expression for τ_w in terms of the wave height

$$\tau_w = \frac{\rho g f_w H^2}{8 h} \quad (15)$$

[28] Then, given equation (12) for the limiting wave height, which applies to the case of **incident wave height** H_i impinging on an intertidal flat with uniform slope β , we can deduce that τ_w at any given stage of the tide must be maximum at some middepth on the intertidal flat. Specifically, $\tau_{w,\text{cross-flat-max}}$, the cross-flat-maximum wave-induced bed shear stress at any given stage of the tide, occurs at the seaward limit of the **zone of wave saturation** where the depth is

$$h_s = H_i / \left(\frac{15\pi \beta}{4 f_w} \right) \quad (16)$$

and at that depth

$$\tau_{w,\text{cross-flat-max}} = \frac{\rho g f_w 15\pi \beta}{8 \cdot 4 f_w} H_i \quad (17)$$

[29] Shoreward of h_s , in the zone of wave saturation, τ_w decreases in proportion to the water depth as

$$\tau_w = \left(\frac{\rho g f_w}{8} \right) \left(\frac{15\pi \beta}{4 f_w} \right)^2 h \quad (18)$$

and seaward of h_s , τ_w is inversely proportional to the water depth as

$$\tau_w = \left(\frac{\rho g f_w}{8} \right) \left(\frac{H_i^2}{h} \right) \quad (19)$$

[30] These features are illustrated by Figure 1, which shows the distribution of H and τ_w across a profile with uniform slope and quadratic bottom friction at different stages of the tide and for different values of incident wave height H_i impinging on the seaward end of the profile. Waves are assumed to be shallow water everywhere across the profile. Figure 1a shows water level across the profile for six different stages of the tide; the zero datum is the high-water level. Figure 1b shows the water depth across the profile for the six stages of the tide. Figure 1c shows wave height across the profile for the six stages of the tide. The incident wave height at each stage of the tide is the same. This may occur if the fetch beyond the intertidal flat is large relative to the width of the intertidal flat, in which case the covering and

GREEN AND COCO: WAVE-DRIVEN SEDIMENT TRANSPORT

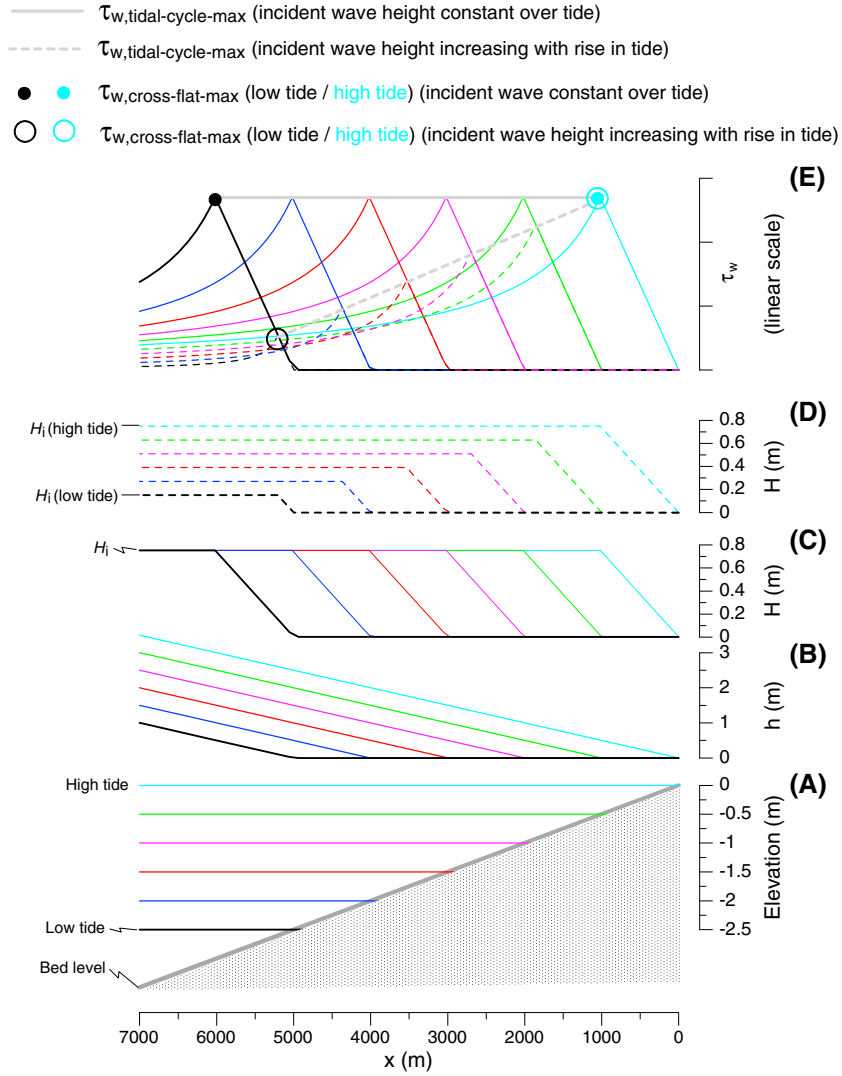


Figure 1. Distribution of H and τ_w across a profile with uniform slope and quadratic bottom friction at different stages of the tide and for different values of incident wave height H_i impinging on the seaward end of the profile. (a) The seabed (heavy grey line) and water level at six different stages of the tide (colored lines). The black line depicts low-tide water level and the cyan line is high-tide water level. (b) Cross-flat distribution of water depth at the six different stages of the tide. (c) Cross-flat distribution of wave height at the six different stages of the tide; incident wave height at each stage of the tide is the same. (d) Same as Figure 1c except that the incident wave height increases (arbitrarily) as the tide rises. (e) Cross-flat distribution of bed shear stress τ_w at the six different stages of the tide. The solid lines refer to the case in which the incident wave height at each stage of the tide is the same. The dashed lines refer to the case in which the incident wave height increases as the tide rises. The solid grey line shows the cross-flat distribution of $\tau_{w,tidal-cycle-max}$ between the seaward limit of the zone of wave saturation that exists at low tide and the seaward limit of the zone of wave saturation that exists at high tide for the case in which the incident wave height at each stage of the tide is the same. The dashed grey line shows the same for the case in which the incident wave height increases as the tide rises.

uncovering of the flat by the tide will not add significantly to the fetch. A further assumption is that the wave height seaward of the zone of wave saturation is constant, i.e., $H=H_i$ for $h>h_s$, where $h_s=H_i/[(15\pi/4)(\beta/f_w)]$ (equation (16)). This situation can occur when the change in wave height due to shoaling is exactly balanced by the change in wave height due to frictional dissipation by bottom friction. Inside the zone of wave saturation ($h<h_s$), wave height is directly proportional to water depth, $H=h(15\pi/4)(\beta/f_w)$.

Figure 1d also shows wave height across the profile for the six stages of the tide, except in this case the incident wave height increases (arbitrarily) as the tide rises. Figure 1e shows the cross-flat distribution of bed shear stress τ_w for the six stages of the tide. For $h>h_s$, τ_w is inversely proportional to the water depth (equation (19)) and for $h<h_s$, τ_w is directly proportional to the water depth (equation (18)). Hence, there is a cross-flat-maximum wave-induced bed shear stress $\tau_{w,cross-flat-max}$ (equation (17)) that occurs at a middepth,

which is the depth at the seaward limit of the wave-saturation zone. With H_i constant over the tidal cycle, both h_s and $\tau_{w,cross-flat-max}$ also remain constant as the tide rises from low tide; however, the location on the flat where they occur is translated landward (solid colored lines; Figure 1e). Hence, between the seaward limit of the zone of wave saturation that exists at low tide and the seaward limit of the zone of wave saturation that exists at high tide, the tidal-cycle-maximum wave-induced bed shear stress, $\tau_{w,tidal-cycle-max}$, will be uniform. This is shown in Figure 1e by the solid grey line. In contrast, with H_i increasing as the tide rises, both h_s and $\tau_{w,cross-flat-max}$ increase as the tide rises (dashed colored lines; Figure 1e). As a result, $\tau_{w,tidal-cycle-max}$ increases from a minimum value at the seaward limit of the low-tide wave-saturation zone to a maximum value at the seaward limit of the high-tide wave-saturation zone. This is shown in Figure 1e by the dashed grey line. In this way, the basin geometry exerts a significant control on the pattern of wave-induced bed shear stress on the intertidal flat.

[31] Finally, note that essentially the same cross-flat pattern in τ_w will occur when the change in wave height due to shoaling exceeds the change in wave height due to frictional dissipation by bottom friction. That is, τ_w will still acquire a maximum value at a middepth, but compared to the case of shoaling balanced by dissipation, h_s will be greater, and therefore the wave-saturation zone will be wider, and τ_w will rise to a larger value of $\tau_{w,cross-flat-max}$.

[32] *Carniello et al.* [2005] computed the spatial distribution of the bed shear stress $\tau_{t,wc}$ for the Venice Lagoon from the tidal-current and wind-wave fields simulated by their coupled wind wave-tide model. Here $\tau_{t,wc}$ is the total bed shear stress due to the combined action of waves and currents and is given as the vector sum of the wave component of the stress and the current component of the stress, both of which are enhanced over their respective pure-flow values by nonlinear interaction in the boundary layer. As expected, they found that the magnitude and distribution of $\tau_{t,wc}$ was extremely sensitive to the water depth; in deep channels, where the bed shear stress was high due to the tidal currents, the waves barely affected the bed stress, but on the tidal flats bed stress was dominated by waves. *Carniello et al.* deduced from simulations at several specific stages of the tide that the tidal-flat-maximum value of $\tau_{t,wc}$ occurred at intermediate water depths, since waves were smaller in shallower water, and in deeper water the wave-orbital motions at the bed were reduced by depth attenuation. This result is at least qualitatively consistent with Figure 1, derived from the considerations of *le Hir et al.* [2000], which in turn are based on much more restrictive assumptions.

[33] *Fagherazzi et al.* [2006] demonstrated that τ_w reaches a maximum at an intermediate water depth, confirming that τ_w is limited in both shallower water, because of dissipative processes, and deeper water, because of water-column attenuation of wave-orbital motions. Furthermore, the relationship between τ_w and water depth was shown to be a function of the fetch, with the maximum in τ_w becoming greater and shifting toward greater water depths as the fetch increases. They attributed this to wave height increasing with increasing fetch

(for any given wind speed). However, in deriving these relationships, they assumed a constant, arbitrary wave period, thus neglecting the dependence of wave period on the fetch.

[34] *Mariotti and Fagherazzi* [2013b] provided a fuller account of the relationship between τ_w and water depth by accounting for wave-period effects. Theirs is also a fuller account than the analysis above based on *le Hir et al.* [2000], in which only simple propositions concerning the change of wave height with fetch are made.

[35] In essence, there is a wave-period effect because wave period monotonically increases with fetch and water depth, thereby augmenting τ_w through a reduction in the water-column attenuation of the wave-orbital motions, which results in a shift of the maximum value of τ_w to deeper water. Compared to *Fagherazzi et al.*, *Mariotti and Fagherazzi* found that this results in a much stronger dependence of the relationship between τ_w and water depth on fetch, with the rate of change of τ_w with water depth either side of the maximum value of τ_w showing a strong fetch dependence (Figure 2). The decay of τ_w with increasing water depth to the right of the maximum value of τ_w (Figure 2) is gradual for long fetch and rapid for short fetch, which difference is explained by the coupled effects of water depth, wave height, and wave period. The effect of wind speed is similar to that of fetch: greater wind speeds increase the maximum τ_w and the depth corresponding to the maximum τ_w and slow the decay of τ_w with increasing depth beyond the depth of the maximum τ_w .

[36] *Mariotti and Fagherazzi* also showed that for small water depths (<1 m) and strong winds (>15 m/s), τ_w has almost no dependence on fetch but for larger water depths τ_w is strongly dependent on fetch (Figure 2). For fixed wind speed and water depth, τ_w monotonically increases with fetch, tending asymptotically to the maximum value that is obtained when the waves become depth limited. In shallow water, τ_w grows faster toward its maximum value as the fetch increases. For instance, for a water depth of 0.5 m, the maximum is obtained at a fetch of less than 1 km under a 20 m/s wind, but for a water depth of 3.5 m, the maximum has still not quite been reached at a fetch of 20 km (Figure 2). *Mariotti and Fagherazzi* noted that the wind speed also influences the rate at which τ_w grows toward its maximum value as the fetch increases. So, for a fixed fetch, τ_w may be higher in shallower water than in deep water if the wind speed is small, while the opposite occurs if the wind speed is high.

[37] *Mariotti and Fagherazzi* pointed out that large differences in the relationship between τ_w and depth occur for fetches between 2.5 and 20 km, which are typical of estuarine intertidal flats. If the fetch is large, then during storms, τ_w may be high at all water depths. However, if the fetch is small, then τ_w may peak at an intermediate depth. *Mariotti and Fagherazzi* examined the implications of this finding for the Willapa Bay mudflats where the fetch presented to the dominant wind in summer is short (2.5 km) compared to the summer fetch (5–10 km). To explore the cross-flat distribution of wave forcing of sediment resuspension, they defined a wave erosion work E_w as a function of τ_w (which itself is a function of water depth, fetch, and wind speed), a critical bed shear stress for erosion, the frequency of occurrence

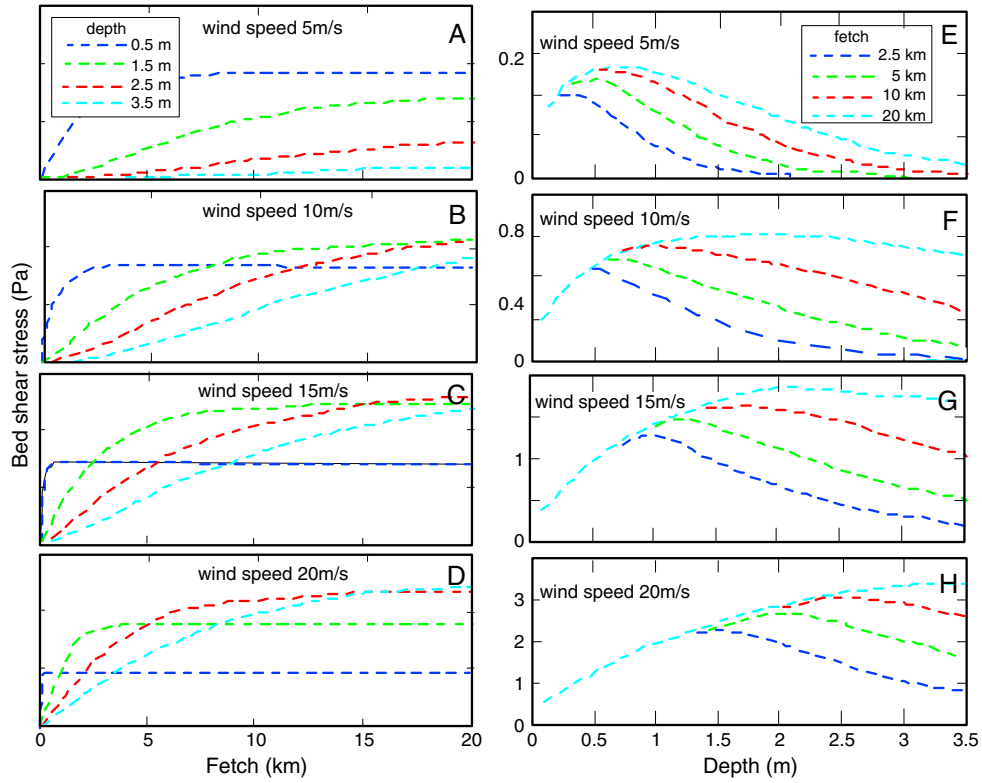


Figure 2. Wave-induced bed shear stress calculated for the Venice Lagoon by the SWAN model as a function of (a–d) fetch and (e–h) depth for wind speeds 5 m/s (Figures 2a and 2e), 10 m/s (Figures 2b and 2f), 15 m/s (Figures 2c and 2g), and 20 m/s (Figures 2d and 2h). This is redrawn from *Mariotti and Fagherazzi* [2013b] with permission from Elsevier.

of water depth, and the frequency of occurrence of wind speed. Using E_w , they were able to estimate, for different fetches, the water depth at which sediment resuspension by waves is the most effective. They found that for short fetches (2.5 km), E_w is maximum at water depths between 0.5 and 1 m. They interpreted this as meaning that sediment resuspension is greatest when tide levels are near mean sea level (water depths are about 1 m); at high tide and during storm surges, erosion is limited. Conversely, for longer fetches, the erosion work occurs over a wider range of depths (0.5–2.5 m), which means that resuspension also occurs at high water levels (astronomical tides or storm surges) when the fetch is long.

[38] Basin planform and **hypsoetry** are in fact strong controls on wave generation and wave-induced bed shear stress. *Sanford* [1994] established a link between wind climate and basin geometry by drawing resuspension “response diagrams” that plotted τ_w as a function of wind speed and wind direction for given sites. By superimposing estimates of the critical stress for initiation of sediment motion, the response diagrams were used to assess the importance of wave resuspension. *Fagherazzi and Wiberg* [2009] were able to show how water depth and fetch covaried with changes in water level in shallow tidal basins in the Virginia Coastal Reserve (USA) and, from that, how wave height and wave-induced bed shear stress also varied. Their results are reproduced in Figure 3, which shows how average (over the basin) area, fetch, depth, wave height, and τ_w vary with water level. They argue that their results are typical of shallow,

microtidal to mesotidal intertidal basins that are characterized by deep channels, shallow tidal flats, and emergent salt marshes. Referring to Figure 3, different regimes may be identified. For water level rising from the minimum level to **MLLW** (mean lower low water), when water is present only in subtidal channels, the basin-average fetch and water depth both increase monotonically, and the wave height also increases as a result. However, the increase in wave height is counteracted by the increasing depth attenuation of wave-orbital motions, with the result that the basin-average τ_w remains approximately constant. For water levels rising between MLLW and **MSL** (mean sea level), which results in the covering of the lower portions of intertidal flats, the depth attenuation of the wave-orbital motions associated with the increasing depth increases faster than the increase in wave height associated with the increasing fetch and water depth. The result is that the basin-average τ_w reduces. *Fagherazzi and Wiberg* call this the “depth-driven regime” (which they associate with tidal flats) since, on average, depth plays a critical role in determining τ_w , with an inverse relationship between the two. Figure 3 also shows how waves affect salt marshes, which lie between MSL and **MHHW** (mean higher high water). As the tide rises in this elevation range, the fetch increases rapidly as marshes are flooded, but the water depth does not increase as quickly, with the result that τ_w increases much faster than does wave height. During storm surges, when the water level rises above MHHW, fetch does not change and only water depth increases.

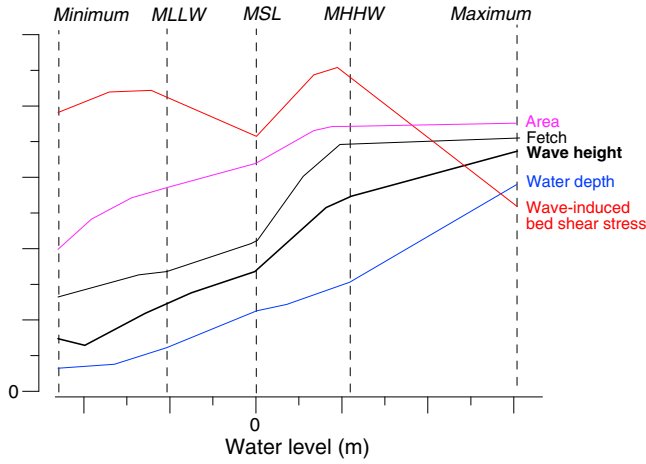


Figure 3. Basin area and average fetch, depth, wave height, and wave-induced bed shear stress as a function of water level. The left-hand axis is linear, with zero at the base of the axis. “Average” is average over the entire estuarine basin. Mean sea level (MSL) is 0 m. MLLW is mean lower low water and MHHW is mean higher high water. The data are for a system of shallow tidal basins, with a particular wind speed and direction. Redrawn from *Fagherazzi and Wiberg [2009]* with permission from the American Geophysical Union.

Hence, τ_w reduces, which implies reduced erosion of marshes (but not at the marsh edges, which waves directly impact).

2.4.2. Temporal Variation in Bed Shear Stress

[39] The variation in τ_w over the tidal cycle at any point on the intertidal flat can be deduced by taking vertical slices through Figure 1.

[40] *le Hir et al. [2000]* showed that there are two patterns of temporal variation (see their Figure 13) for the case in which the incident wave height H_i remains constant as the tide rises from low tide. As pointed out above, this may occur when the fetch beyond the intertidal flat is large relative to the width of the intertidal flat. Figures 4a–4d down the left-hand side show this case; in addition to constant incident wave height, for simplicity, wave shoaling is assumed to be exactly balanced by frictional dissipation seaward of the wave-saturation zone.

[41] Figure 4a shows the variation over the tidal cycle of the water level, where the zero datum is (arbitrarily) the high-water level. Figure 4b shows the variation over the tidal cycle of water depth at six locations on a profile with uniform slope, where the locations are given as distance offshore (positive) and $x=0$ at the landward end of the profile. The water depth goes to zero when the seabed is exposed by the retreating tide, and vice versa. Figure 4c shows the variation over the tidal cycle of wave height at each of the six locations on the profile; the incident wave height is shown as the heavy, dashed, grey line. Because wave shoaling is assumed to be exactly balanced by frictional dissipation seaward of the wave-saturation zone, wave height is equal to the incident wave height when $h > h_s$ and when $h < h_s$ wave height is proportional to the water depth (equation (12)). Note that the locations $x = 1000$ m and $x = 500$ m are in the zone of wave saturation throughout the tidal cycle, indicated by the

fact that at these locations, H is always less than H_i . Figure 4d shows the variation over the tidal cycle of τ_w at each of the six locations on the profile. For the two locations toward the top of the flat that are always inside the zone of wave saturation (i.e., $x = 1000$ m and $x = 500$ m), τ_w is always proportional to the water depth (equation (18)), with $\tau_{w,tidal-cycle-max}$ therefore occurring once per tidal cycle, at high tide (see Figure 4d). For the other locations, τ_w is proportional to h only early in the flood and late in the ebb when $h < h_s$ and the location of interest is therefore in the wave-saturation zone. Between early flood and late ebb when $h > h_s$ (this includes high tide), τ_w is proportional to $(1/h)$ (equation (19)). Hence, $\tau_{w,tidal-cycle-max}$ occurs twice every tidal cycle, once between low tide and high tide on the flooding tide, and a second time between high tide and low tide on the ebbing tide (see Figure 4d). Furthermore, moving down the intertidal flat (i.e., increasing x), the two occurrences of $\tau_{w,tidal-cycle-max}$ (one on the flood and one on the ebb) increasingly converge on low tide; conversely, moving up the intertidal flat (i.e., decreasing x), the two occurrences of $\tau_{w,tidal-cycle-max}$ increasingly converge on high tide (see Figure 4d).

[42] When the incident wave height varies in phase with the tide, which is likely to be the case when the fetch beyond the intertidal flat is small relative to the width of the intertidal flat, more complicated temporal patterns result. One such pattern is shown in Figures 4e–4h down the right-hand side, in which H_i rises to a maximum at high tide when the fetch is greatest. (The incident wave height is shown in Figure 4g as the heavy, dashed, grey line.) Note that as in the panels on the left-hand side of the figure, the two locations toward the top of the flat, $x = 1000$ m and $x = 500$ m, are always inside the zone of wave saturation, which results in there being just one peak in τ_w , which occurs at high tide (Figure 4h). At the locations seaward of $x = 1000$ m, which pass out of and in to the zone of wave saturation as the tide rises and falls, respectively, there are two peaks in τ_w , one on the flood and one on the ebb, for the same reasons that there are two peaks in the constant incident-wave case. However, there is also now a third peak in τ_w , which occurs at high tide. This occurs because the rate of fetch extension has been chosen in this case such that H_i^2 increases faster than h as the tide rises (see equation (19)). Depending on how the fetch changes with the change in the tide, the high-tide peak in τ_w may dominate, which again shows how basin geometry exerts a significant control on patterns of wave-induced bed shear stress.

[43] *Dolphin and Green [2009]* compared measurements of tidal-cycle variation in $U_{w,b}$ at two locations on a mesotidal intertidal flat (Wiroa Island, Manukau Harbour, New Zealand) that are broadly consistent with the above picture. At this site the wave height varied significantly over the tidal cycle in response to a change in fetch (wave height greatest at high tide). At the shallower location ($h = 1$ m at high tide), $U_{w,b}$ (and therefore τ_w) varied in phase with the water depth, with $U_{w,b}$ peaking once at high tide, suggesting that this location was submerged in the wave-saturation zone throughout the tidal cycle. Conversely, at the deeper location ($h = 2$ m at high tide), $U_{w,b}$ was smallest at high tide, and there were two peaks per tidal cycle in $U_{w,b}$, one just after

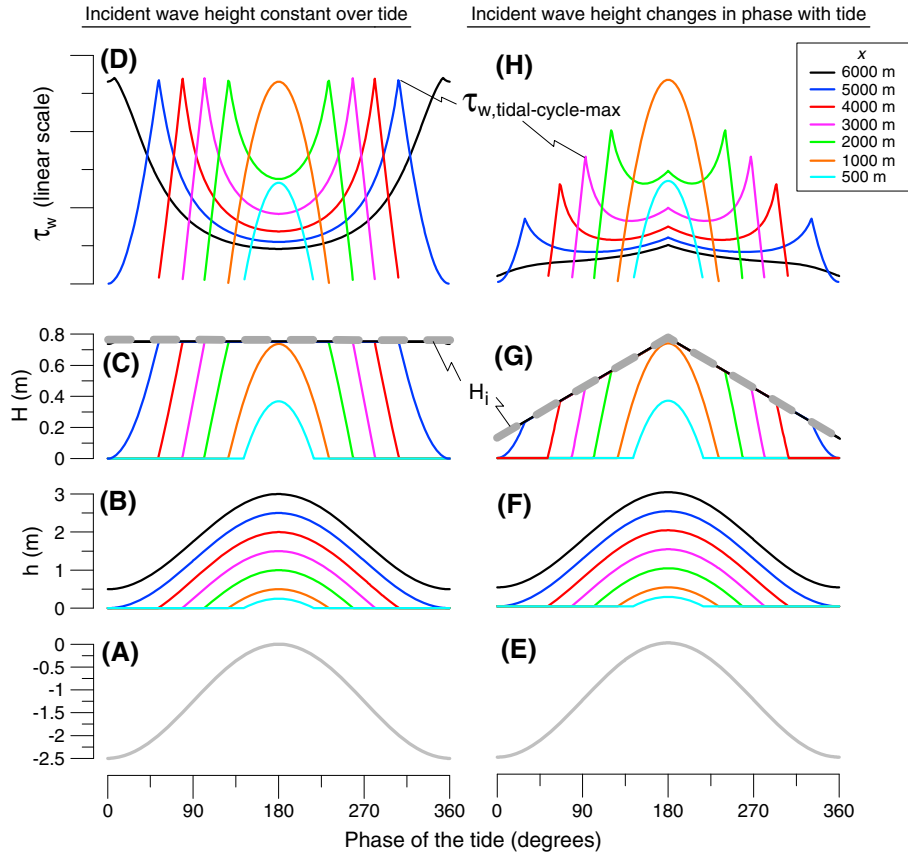


Figure 4. Variation over the tidal cycle in H and τ_w for different locations on a profile with uniform bottom slope and quadratic bottom friction. The locations are given as distance offshore (positive) where $x=0$ at the landward end of the profile (see Figure 1). (a–d) For the case in which the incident wave height H_i is constant over the tidal cycle. (e–h) For case in which the incident wave height varies in phase with the tide. At all stages of the tide $H=H_i$ between the outer end of the profile and the seaward limit of the zone of wave saturation where the water depth is h_s . This implies that the change in wave height due to shoaling is exactly balanced by the change in wave height due to dissipation by bottom friction. (Figures 4a and 4e) Water level. (Figures 4b and 4f) Water depth. (Figures 4c and 4g) Wave height. (Figures 4d and 4h) Wave-induced bed shear stress. See text for detailed explanation of figure.

the sensors were covered on the flooding tide and one just before the sensors were uncovered on the ebbing tide. It is quite difficult to interpret this kind of data: for one thing, the measurements were truncated as the sensors emerged from the water column before the water arrived at (on the flooding tide) and left from (on the ebbing tide) the measurement sites. Nevertheless, inserting typical values for β and f_w (0.03 and 0.001, respectively) into equation (12) yields $[H/h]_{\text{lim}} \approx 0.4$, which equates to $h_s \approx 1$ m for the observed wave heights. This value of h_s places the shallower site in the zone of wave saturation at high tide, where the theory says τ_w should peak at high tide, and it places the deeper site seaward of the zone of wave saturation, where the theory says τ_w should attain a minimum value at high tide.

3. SEDIMENT RESUSPENSION BY WAVES

3.1. Initiation of Sediment Motion—Waves Versus Currents

[44] Experimental observations confirm that a division between waves and currents, in the context of sediment

transport, is meaningful. For example, *Schoellhamer* [1995] showed that (episodically occurring) waves that generated bottom orbital speeds of 15–20 cm/s dominated sediment resuspension at two depths (1.5 m and 4 m), even though mean currents (periodically) attained speeds of 15 cm/s (Figure 5). *Christiansen et al.* [2006] used regression analyses to show that suspended-sediment concentration was controlled more by the wave-induced bed shear stress than by the current-induced stress on a microtidal intertidal flat in the Ho Bugt in the Danish Wadden Sea (high-tide water depths 1–1.5 m). *de Jonge and van Beusekom* [1995] looked explicitly at the relative roles of waves and currents in the Ems-Dollard estuary and found, again using regression analyses, that they both contribute to resuspension of bed sediments (and associated **microphytobenthos**) but to different degrees. For instance, a doubling of wind speed caused a much greater increase in suspended-sediment concentration on intertidal flats than a corresponding doubling in tidal-current speed, leading them to conclude that the “effect of wind on the suspended matter concentration appears to be predominant”. Differences in the slope of the linear relationship between

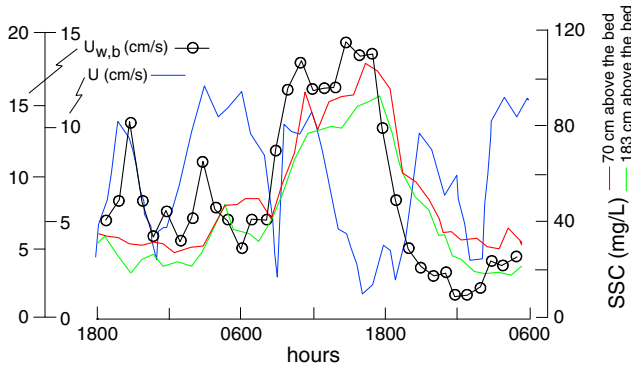


Figure 5. Mean current speed, wave-orbital speed at the bed, and suspended-sediment concentration at two levels above the bed during the passage of a storm, Old Tampa Bay, 1990. Redrawn from *Schoellhamer* [1995] with permission from Elsevier.

suspended-sediment concentration and wind speed in different parts of the estuary were interpreted as being due to differences in bed-sediment composition, with finer sediment being more easily resuspended. *de Jonge and van Beusekom* also distinguished the relative roles of currents and waves on intertidal flats compared to in channels, showing that wind has a direct effect on suspended-sediment concentration in shallow (<2 m) water on the intertidal flats but has no direct effect on concentrations in the deep (7–25 m) main channels, from which they inferred that tidal flats are the main source of resuspended mud when it is windy. Using wave and current measurements in the analytical model of *van Rijn* [1990], *Janssen-Stelder* [2000] estimated the wave and current components of the combined bed shear stress at a location just seaward of salt marshes (water depth <1 m, but up to 1 m deeper in a strong onshore wind). *Janssen-Stelder* found that during calm weather, the current component just exceeded the wave component, but during storms the combined stress increased and waves contributed most (up to 81%) of the combined stress and at those times suspended-sediment concentration was as much as 3 times greater than in calm weather.

[45] *Green and MacDonald* [2001] showed that waves—not currents—initiate sediment transport on a sandy microtidal intertidal flat (Okura estuary, New Zealand) (high-tide water depth 2.5–3 m). They plotted data against the dimensionless wave-induced skin friction θ'_w on one axis and the dimensionless current-induced skin friction θ'_c on the other axis, where

$$\theta'_w = \left(0.5\rho f'_w U_{w,b}^2\right) / [(\rho_s - \rho)gD] \quad (20)$$

with f'_w the skin-friction wave friction factor, ρ_s the sediment density, and D the sediment grainsize. θ'_c is analogous with the wave-orbital speed replaced by a current speed and the wave friction factor replaced by a current-related **drag** coefficient. *Green and MacDonald* found that θ'_c never exceeded the theoretical dimensionless skin friction for initiation of motion θ'_{crit} but θ'_w did, and there was a good separation around θ'_{crit} of bursts in which sediment was being resuspended and bursts in which there was no resuspension (Figure 6). *Green* [2011] examined the onset of resuspension

(high-tide water depth 1.25 m) from a wave-by-wave (as opposed to burst averaged) point of view and showed that resuspension was initiated when ~40% of the maximum wave-orbital speeds in a measurement burst exceeded the critical orbital speed for initiation of motion as predicted by *Komar and Miller* [1973, 1975], which includes a dependence on wave period:

$$\frac{\rho U_{w,b,crit}^2}{(\rho_s - \rho)gD} = 0.21 \left(\frac{A_{b,crit}}{D}\right)^{1/2} \quad (21)$$

[46] Here $U_{w,b,crit}$ is the critical wave-orbital speed at the bed for initiation of sediment motion, and $A_{b,crit}$ is the seabed orbital semiexcursion at the initiation of sediment motion. In contrast, there was no obvious control on resuspension by the mean (tidal) current. *Green* interpreted the data as suggesting that suspended sediment resulted from the release of fine silt (<20 μm) from the seabed fine-sand (100–200 μm) matrix by wave-generated fluid forces acting on the particles in the fine-sand matrix. *Green* arrived at this conclusion by noting that the data indicated a value for θ'_w of ~0.06 at the onset of resuspension, which is approximately the critical dimensionless skin friction for initiation of granular sediment transport on a flat, unconsolidated bed of sediment of grainsize 0.2 mm [*Graf*, 1971; *van Rijn*, 1990].

[47] *Booth et al.* [2000] used linear wave theory to develop a model of sediment resuspension in terms of wind speed. Their model was based on the proposition that when the water depth is less than half the surface-wave wavelength, wave energy is transferred to the bottom sediments, which may cause resuspension. They used linear wave theory to calculate, for any given water depth, a critical wave period T_{crit} , above which resuspension is expected. Then, using formulations in *U.S. Army Coastal Engineering Research Center* [1984] that relate wave period to wind speed, fetch,

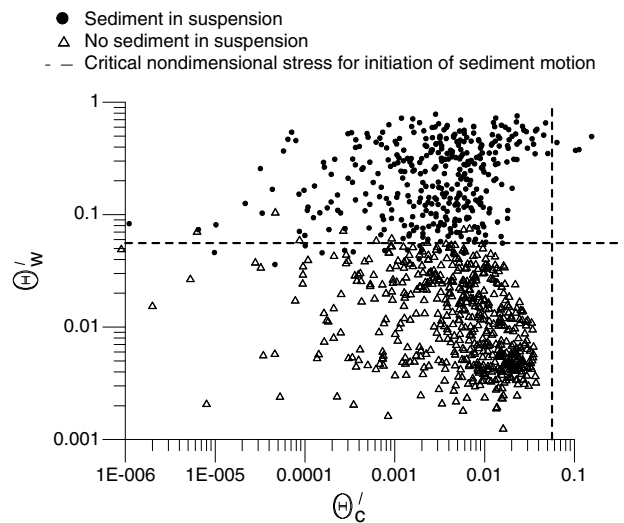


Figure 6. Scatterplot of θ'_w versus θ'_c . $\theta'_{crit} = 0.056$ applies to the bed sediment, which was noncohesive, with grainsize 0.15 mm. Symbols are filled in if the sediment was observed to be in motion and open if not. Redrawn from *Green and MacDonald* [2001] with permission from Elsevier.

and duration, they found an expression for the critical wind speed $U_{\text{wind,crit}}$ for the initiation of sediment resuspension:

$$U_{\text{wind,crit}} = \left[1.2 \{ 4127 (T_{\text{crit}}^3 / F) \}^{0.813} \right] \quad (22)$$

[48] The model was validated with water-column turbidity satellite imagery of Barataria Bay (Louisiana, USA).

[49] As noted above, where currents are also present, they interact in the boundary layer with waves to nonlinearly enhance the bed shear stress [Soulisby *et al.*, 1993]. *Green et al.* [1997] showed evidence for the effects of wave-current interaction on an intertidal flat. The seabed **hydraulic roughness** Z_0 , which is related to the steady-flow drag coefficient through the **law of the wall**, was found to be constant throughout the tidal cycle when there were no waves, but in the presence of waves Z_0 was enhanced and varied directly with the ratio $U_{\text{w,b}}/U$, which is characteristic of wave-current interaction. Here U is the steady (tidal) current speed. The time-averaged bed shear stress was found to be as much as 3.75 times greater when waves were present. *Bricker et al.* [2005] also approached this problem from the perspective of the extra drag felt by the mean flow in the presence of waves. They showed that for a shallow site in San Francisco Bay, the steady-flow drag coefficient increased as $U_{\text{w,b}}/U$ increased, and the steady-flow drag coefficient was an order of magnitude greater than the pure-current value when the mean current velocity was much less than the near-bed orbital velocity.

[50] *Wright et al.* [1992] identified a background signal of low-amplitude swell in the broad, flat subtidal areas (“stem plains”) of the lower Chesapeake Bay (USA) (depth 11–12 m), which added to the currents to raise the hydraulic roughness sensed by the mean flow. They noted that the wave motions were too weak on their own to resuspend bed sediments but that they could tip the balance in favor of resuspension at times. *Schoellhamer* [1995] looked for an effect of wave-current interaction on sediment resuspension in microtidal Old Tampa Bay (Florida) but was unable to distinguish between any possible effect and uncertainties associated with estimation of wave parameters and the wave friction factor. Other studies though have provided evidence of the importance of wave-current interaction. For instance, *Talke and Stacey* [2003] found that the bed stress and associated drag coefficient on an intertidal flat in San Francisco Bay increased significantly (compared to the value under pure tidal currents) when waves were present, which they attributed to wave-current interaction. In this case, waves were different combinations of locally generated wind waves and remotely forced ocean swell that propagated into the Bay from the adjacent ocean, experiencing extensive dispersion, dissipation, and transformation as they did so. *Talke and Stacey* noted that although ocean waves contributed only around 10% of the kinetic energy at their inner Bay, intertidal-flat field site over a 2 week **spring-neap** cycle, they may still have been important to the sediment dynamics, since the bed stress was greatly enhanced by interaction between the ocean swell and the tidal current. In addition, they pointed out that when the bed shear stress in the absence of waves is close to critical for sediment

motion, even the small additional stress by ocean swell can tip the flow from being unable to resuspend sediment to being able to resuspend sediment.

[51] *Verney et al.* [2007] found that in the presence of waves, $\tau_{\text{t,wc}}$ on the intertidal Vasière Nord mudflat at the mouth of the macrotidal Seine River estuary (France) was twice to 1 order of magnitude higher than the bed shear stress attributable to the tidal current in the absence of waves. The latter was estimated from the turbulent kinetic energy, and $\tau_{\text{t,wc}}$ was estimated using *Soulisby’s* [1995] **parametric** wave-current interaction model:

$$\tau_{\text{t,wc}} = \sqrt{(\tau_{\text{c,wc}} + \tau_{\text{w}} \cos \psi)^2 + (\tau_{\text{w}} \sin \psi)^2} \quad (23)$$

where

$$\tau_{\text{c,wc}} = \tau_{\text{c}} \left(1 + \left\{ 1.2 \left(\frac{\tau_{\text{w}}}{[\tau_{\text{w}} + \tau_{\text{c}}]} \right)^{3.2} \right\} \right) \quad (24)$$

[52] Here $\tau_{\text{c,wc}}$ is the current component of the total combined wave-current bed shear stress $\tau_{\text{t,wc}}$, which is enhanced relative to the pure-current bed shear stress τ_{c} , and ψ is the angle between the waves and the current. Deposition (inferred from bed altimetry data) was found to occur when $\tau_{\text{t,wc}}$ fell below 0.8 N/m^2 , and the deposition rate increased with decreasing $\tau_{\text{t,wc}}$. Conversely, erosion began when $\tau_{\text{t,wc}}$ exceeded 1 N/m^2 , which *Verney et al.* noted is in the upper range of critical erosion shear stress (0.1 to 1.5 N/m^2) measured by *Mitchener and Torfs* [1996] for newly deposited muddy bed sediments. Furthermore, there was a relationship between erosion rate and bed-sediment properties, in that the erosion rate was greater shortly after periods of deposition when the surface sediments were young, unconsolidated, and had a low bulk density. *Nowacki and Ogston* [2012] observed an increase in bed shear stress during windy periods compared to during calm periods in a shallow channel on the mesotidal Willapa Bay (Washington, USA) intertidal flats, which they attributed to (an unknown combination of) wind-driven flow and wave-orbital motions adding to and interacting with the tidal current. They noted that the additional bed stress so generated was available to erode the bed sediment, although it was not always capable of actually doing so.

[53] *D’Alpaos et al.* [2013] analyzed the statistical properties of resuspension events due to $\tau_{\text{t,wc}}$, the total bed shear stress due to the combined action of waves and currents, in the Venice Lagoon. Their work was motivated by the recognition that wind waves are critically important to the biomorphodynamic evolution of tidal landscapes (see section 5 of this review) and that to reduce computing cost, efficient landscape models could employ a theoretical framework for representing wind-wave-induced resuspension events and accounting for their erosional effects. For this work, they used the fully coupled wind wave-tide model of *Carniello et al.* [2005, 2011] to simulate a single representative meteorological year and analyzed the peaks in predicted combined wave-current bed shear stress over a resuspension threshold.



Figure 7. A turbid fringe. Photo by M. Green.

D'Alpaos et al. showed that τ_c was not large enough to resuspend sediments on the intertidal flats but that the bed shear stress under waves combined with currents was. Furthermore, the effect of the nonlinear interaction between the waves and the currents, indicated as the difference $\tau_{t,wc} - (\tau_c + \tau_w)$, was as large as 10% of $\tau_{t,wc}$. Also, although the wave-induced bed shear stress was larger than that due to the current, the current nevertheless was significant in that it modulated $\tau_{t,wc}$ and increased peak values of bed shear stress by up to 30%.

[54] *D'Alpaos et al.* found that at most locations in the lagoon, the **interarrival time** between resuspension events was exponentially distributed, with the distribution being characterized by a parameter λ such that $1/\lambda$ is the mean value of the interarrival time. This is the defining characteristic of a **Poisson process**. The exceptions were on salt marshes, where the reduced water depth prevented exceedance of the threshold, and in tidal channels, where exceedances did occur but were related to tidal currents, which cannot be represented by a Poisson process. Interarrival times were large in areas that were leeward of obstacles (e.g., spits, islands, and structures), and they were small where the fetch was unlimited and the water depth was about 1.5 m relative to mean sea level, which is where wave-induced bed shear stress is known to be maximum (compared to water both deeper and shallower). Event intensity and event duration were also found to be exponentially distributed, each with its own characteristic value of λ . As was the case for the interarrival time, λ for event intensity and λ for event duration were also spatially distributed, being linked to sheltering and local water depth. Large intensities and long durations were found in the southern part of the lagoon, where recent observations have revealed a significant erosional trend.

3.2. Temporal and Spatial Patterns of Wave Resuspension

[55] Where waves are the primary control on resuspension of intertidal-flat bed sediments, we can expect that spatial and temporal patterns in resuspension will follow spatial and temporal patterns in $U_{w,b}$ and τ_w . Experimental observations confirm the expectation. For instance, *Janssen-Stelder* [2000] described a characteristic temporal variation in suspended-sediment concentration (SSC) over the tidal cycle when waves were present, with concentration peaks occurring at the beginning of the flooding period and at the end of the ebbing period, when wave-orbital motions at the bed were strongest. *Green and Coco* [2007] showed SSC under waves decreasing with increasing water depth, with two peaks in SSC per tidal cycle, one just after low tide on the rising tide, and another just before low tide on the falling tide, also coinciding with the times of highest $U_{w,b}$. These observations are consistent with the deduction from the model of *le Hir et al.* [2000] that $\tau_{w,tidal-cycle-max}$ occurs twice every tidal cycle (once between low tide and high tide on the flooding tide and a second time between high tide and low tide on the ebbing tide), when the location of interest is not always in the zone of wave saturation (section 2). In contrast to *Janssen-Stelder's* and *Green and Coco's* observations, *Bassoullet et al.* [2000] reported that under wave-dominated conditions on the Brouage mudflat (in the macrotidal Bai de Marennes-Oleron, France), peak mud resuspension due to waves on the elevated part of the intertidal flat occurred once per tidal cycle, around high **slack water**. This is explainable by the model of *le Hir et al.* [2000] if we assume that the location in question is always in the zone of wave saturation, in which case $\tau_{w,tidal-cycle-max}$ is predicted to occur once per tidal cycle, at high water.

[56] Converting to a **Lagrangian** perspective, these kinds of point measurements imply that there is a fringe of turbid, shallow water around the edges of the estuary that sweeps up and down the intertidal flat with the tide and within which SSC is maintained by waves that are capable of penetrating to the bed. The so-called wave-driven “turbid fringe” is a readily noticeable feature of estuaries when it is windy (Figure 7). *Green et al.* [1997] suggested that the high turbidity could be enhanced by turbulence associated with (small) breaking waves, aided by whitecapping under a following wind.

[57] Turbid fringes are also commonly observed when it is calm. For example, *Christie and Dyer* [1998] measured flows and SSC in the leading edge of the water body as it transited the macrotidal Skeffling mudflats (Humber estuary, UK). They found that even in the absence of waves, most resuspension occurred during the first and last half hours of immersion. Maximum flood currents occurred during the first few minutes of immersion, and these resuspended low-density material from the surface of the mudflat, which they presumed had been either deposited during the previous ebb cycle or made available for resuspension by biological activity during the low-tide emersion. The result was a clearly visible, highly turbid fringe confined to water depths less than 30 cm, which was **advected** onshore over the tidal flat. A high-concentration turbid fringe also occurred during the ebb phase in water depths less than 0.75 m, which they attributed to vertical

mixing of high-concentration near-bed suspensions that had formed by settling over the immediately preceding high slack water period. The cross-flat sediment **flux** was found to be maximum in the turbid fringe, with net shoreward transport during the calm conditions, causing deposition and ultimately sediment consolidation on the upper flat.

[58] *Uncles and Stephens* [2000] also observed a calm-weather turbid fringe on the Tavy (subestuary of the Tamar River estuary, UK) intertidal flats, but they attributed it to inundation of sediment-laden waters from the main channel rather than to local resuspension of intertidal-flat sediments. However, *Uncles and Stephens* [2010], also reporting on the Tavy, noted that even relatively light winds cause small breaking waves and associated resuspension in the very shallow leading and trailing edges of advancing and retreating waters, respectively, and that these combine with peak flood and peak ebb tidal currents that occur shortly after immersion and shortly before drying, to enhance the turbid fringe. *Christie et al.* [1999] also noted that the current-induced and wave-induced turbid fringes could add together, with waves adding to the high concentrations at the leading edge of the tide and concentrations decreasing with increasing water depth after that, reaching a minimum at high tide. *Weir and McManus* [1987] attributed zones of recurring high turbidity in the macrotidal Tay estuary (Scotland) to wind-wave resuspension of sediment from intertidal flats, aided by an interaction between waves from the dominant wind direction and the flooding tide. The number and size of the turbid zones were shown to be related to wind direction and strength, and specific source areas were identified. *Ruhl et al.* [2001] used satellite reflectance data to identify zones of high SSC in shallow subembayments of San Francisco Bay associated with wind waves. They found that there was little response of SSC to the strongest winds, which they attributed to the fact that strongest winds occurred during neap tides, when water depths were on average deeper. Wind had more effect during spring tides, which they tentatively attributed to more energetic spring tide currents keeping sediments scoured from the bed by waves in suspension for longer.

3.3. Predictors of Suspended-Sediment Concentration by Waves

[59] Many researchers have used statistical methods to explain and develop predictors of wave resuspension, which are difficult to apply at any location other than the measurement site.

[60] Various formulations of wind speed have been used as the independent variable in regression models. For example, *Gabrielson and Lukatelich* [1985] found that resuspension of bottom sediments accounted for up to 90% of deposition rates in the Peel-Harvey estuary (Western Australia) and deposition rates in turn were correlated with a function of the wind speed raised to the third power, where the function was formulated to account for fetch and duration of the wind above a threshold speed. *de Jonge and van Beusekom* [1995] found that mud resuspension can be described as a linear function of the “effective wind speed,” which they defined

as the wind speed averaged over the three high-water periods preceding sampling. *Dyer et al.* [2000] found a good correlation between suspended-mud concentration and wind speed in the Ems-Dollard estuary (mean depth at high water 2 m) and showed that a wind speed in excess of about 6 m/s causes an increase in tidally averaged SSC. *Ridderinkhof et al.* [2000] showed that temporal variations in tidally averaged fine-grained SSC on an intertidal flat and in a channel in the Dollard Basin of the Ems-Dollard estuary could be explained by the maximum water level and the wind speed and showed that wind speed influences the tidally averaged SSC above the flat much more than in the channel, which confirms the previous distinction between the effectiveness of waves and currents on flats and in channels noted by *de Jonge and van Beusekom* [1995]. Others have used wave parameters in regression models, which make them more generally applicable. For example, *Anderson* [1980] explained SSC in terms of wave height, *Schoellhamer* [1995] correlated suspended-sediment (**noncohesive** silts and fine sands) concentration against wave height, bottom wave-orbital speed, and wave-induced bed shear stress, and *Janssen-Stelder* [2000] found a significant correlation between wave height and SSC (bed sediment 10–50% mud, mean grain size 0.06 mm). *Christiansen et al.* [2006] developed regressions of suspended-sediment concentration C on τ_w of the form $C = A_3 \exp(B_3 \tau_w)$ where A_3 and B_3 are the empirical regression constants.

[61] *Nowacki and Ogston* [2012] plotted suspended-sediment concentration against the combined wave-current bed shear stress $\tau_{t,wc}$ for both a channel and a flat to show that the minimum SSC was higher during windy periods than calm periods and that the minimum SSC was set by $\tau_{t,wc}$. Above the minimum there was a great deal of scatter in the data, which they attributed to the SSC being a result of both local resuspension, which could reasonably be attributed to $\tau_{t,wc}$, and advection of sediment-laden water from elsewhere to the measurement site. The two processes could not be unraveled given the particular experimental design, which is nearly always the case, and which greatly complicates any analysis of local resuspension in terms of local current- and/or wave-induced forces on the bed. An exception is the work of *Green and MacDonald* [2001], who examined resuspension of noncohesive fine sand (mean grain size 0.15 mm) by waves in terms of the time-averaged suspended-sediment reference concentration C_{ref} , which is the suspended-sediment concentration “very close to” the bed (in this case, within 1 cm). They found a strong dependence of C_{ref} on θ'_w , which was also seen by *Green and Black* [1999] in data from a wave-dominated, open-coast shoreface. For $\theta'_w < 0.14$, *Green and Black*'s data clustered on the model:

$$C_{ref} = A_4 \rho_s \theta_w^3 \quad (25)$$

with $A_4 = 0.10$ and for $\theta'_w > 0.14$ the same model described the data but with $A_4 = 0.005$. *Green and Black* found that the data could be collapsed onto the one curve (equation (25) with $A_4 = 0.005$) by making a correction to $U_{w,b}$ (from which θ'_w is estimated; see equation (20)) that accounts for

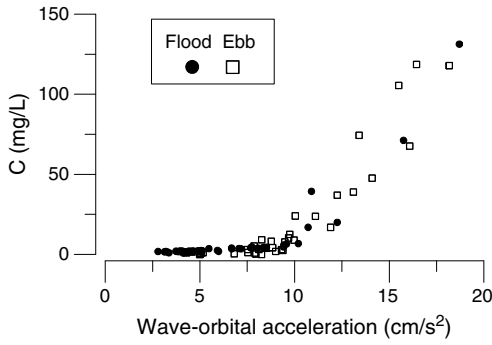


Figure 8. Suspended-fine-silt concentration (time average over 51.2 s, 10 cm above the bed) plotted against wave-orbital acceleration. Redrawn from *Green* [2011] with permission from Elsevier.

contraction of **streamlines** and consequent flow acceleration over the crests of seabed ripples. *Green and MacDonald's* intertidal-flat data were mainly in the regime $\theta'_w > 0.14$ and the data indicated $A_4 = 0.005$.

[62] A strong relationship between wave-orbital acceleration (not speed) and suspended-fine-silt (10 to 20 μm) concentration was found by *Green* [2011] (Figure 8), which implies that wave period exerts a control on sediment resuspension, at least under the very short period waves that were observed (period < 2 s). The skin-friction wave friction factor in equation (20) is usually estimated on the assumption that the boundary-layer flow is hydraulically rough turbulent, in which case f'_w depends on the relative roughness of the seabed expressed as the ratio of grain roughness to wave-orbital semiexcursion (see section 2). *Green*, however, noted that the wave **Reynolds number** RE_w estimated from velocity measurements under the waves at the field site fell well within the range corresponding to a smooth-bed regime ($RE_w < 3 \times 10^5$). In this case f'_w loses its dependence on the relative roughness and instead

$$f'_w = 2/\sqrt{RE_w} \quad (26)$$

where $RE_w = U_{w,b}^2 T / 2\pi\nu$ and ν is the molecular kinematic viscosity of water. By plotting the suspension data against θ'_w calculated using the smooth-turbulent wave friction factor, the acceleration effect was virtually entirely accounted for. An acceleration effect, expressed through a dependence of the wave friction factor on the wave Reynolds number, may not be uncommon. For instance, *Schoellhamer* [1995] also concluded that the bottom boundary layer under locally generated wind waves was transitional between laminar and rough turbulent, based on observed values of A_b/k_b .

[63] To our knowledge, there have been no systematic analyses of vertical profiles of suspended sediment concentration under waves on estuarine intertidal flats, which usually need to be understood in order to estimate suspended-sediment transport. Two possible reasons for this lack of attention come to mind.

[64] First, in the case of very fine sediments, which are easily mixed vertically, profiles of suspended-sediment concentration are likely to be uniform and therefore uninteresting.

Notwithstanding, *Pejrup* [1988] showed vertical profiles of suspended fine sediment from the Danish Wadden Sea that were uniform between 50 and 100 cm above the bed when SSC was low (mean concentration about 80 mg/L) but that became nonuniform (SSC decreased with elevation above the bed) when SSC was higher (mean concentration about 160 mg/L). They attributed this to an effect of **flocculation** on settling speed, which they noted increased with increasing SSC. Nevertheless, most workers calculate horizontal fluxes of fine suspended sediment on the assumption that SSC is uniform and that errors that might arise as a result of this assumption will likely be small or even offset by other uncertainties. An example is the work by *Andersen and Pejrup* [2001], who reported on data from the Danish Wadden Sea.

[65] Second, in the case of coarser sediments, concentrations may reduce very quickly with elevation above the bed, making them very difficult to measure. As an example of the latter, *Green and MacDonald* [2001] found that suspended-sand (particle size 0.15 mm) concentration typically reduced to zero within 5 cm of the bed on an intertidal flat under significant wave heights of around 40 cm.

4. SEDIMENT TRANSPORT

4.1. Suspended-Sediment Transport

[66] Suspended-sediment transport at any particular location may be defined as the integral over the water depth of the product of the suspended-sediment concentration and the horizontal current velocity. The units are mass per time per width of seabed normal to the direction of transport.

[67] At any elevation z above the seabed, the instantaneous current velocity V may be decomposed into a tidal component V_t and a wave component V_w , both of which are vectors. That is, $V(t) = V_t(t) + V_w(t)$ where $\overline{V_w(t)} = 0$ (at least to first order) over a period that is much shorter than the period at which the tidal current varies, and the overbar represents a time average. Similarly, for the suspended-sediment concentration, $C(t) = C_t(t) + C_w(t)$, but $\overline{C_w(t)} \neq 0$ because C_w is a scalar quantity. Then the suspended-sediment transport, or flux, at elevation z averaged over a long time relative to the waves but a short time relative to the tide is given as

$$\overline{V(t)C(t)} = \overline{V_t(t) \cdot C_t(t)} + \overline{V_t(t) \cdot C_w(t)} + \overline{V_w(t)C_w(t)} \quad (27)$$

where the term $\overline{V_w(t) \cdot C_t(t)}$ drops out of the expansion because $\overline{V_w(t)} = 0$. The term $\overline{V_w(t)C_w(t)}$ is the wave transport (or flux) of suspended sediment. This term is a temporal correlation between wave fluctuations in velocity and SSC, which can arise through various mechanisms including interactions of orbital motions with bed forms. The term $\overline{V_t(t) \cdot C_t(t)} + \overline{V_t(t) \cdot C_w(t)} = \overline{V_t(t) \cdot [C_t(t) + C_w(t)]}$ is the tidal transport of suspended sediment which, conceptually, can be thought of as the horizontal advection by the tidal current of the sediment resuspended from the bed by the tidal current and by the wave. The two sources of resuspended sediment, $C_t(t)$ and $C_w(t)$, are usually not distinguished from each other. Most investigators work at these tidal and wave scales; above the tidal scale, waves may be viewed as

efficient estuary-wide agitators of bed sediment, and the sediment so agitated is then transported by slowly varying residual currents

[68] Equation (27) is typically applied to noncohesive sediments, with a different approach taken for **cohesive** sediments. Beds of noncohesive sediment have a granular structure, and the particles that they are composed of do not “cohere” or stick together. As a result, sediment particles erode and deposit individually, and the bed shear stress (be it exerted by waves or currents) acts against the submerged weight of the individual grains to initiate sediment transport. Over a suitable period of time (the passage of many turbulent eddies), there is a local balance—or “equilibrium”—between the erosion and deposition of individual sediment particles. In this case, the time-averaged vertical profile of suspended sediment $C(z)$ may be derived from postulating a balance between the vertical turbulent flux of suspended sediment and the oppositely directed settling flux. The particular form of $C(z)$ then obtained depends on the vertical distribution of sediment diffusivity that is assumed. In contrast, sediment particles that compose a cohesive-sediment bed do cohere, due to electrochemical forces, which confers a certain bulk shear strength to the bed that provides additional resistance against destabilization by the bed shear stress. The bulk shear strength is altered by consolidation of the bed sediment, and because consolidation typically increases with depth in the sediment column due to the increasing sediment overburden, the bed shear strength also increases. This means that the bed shear stress at which erosion begins increases with depth in the bed sediment, making the sediment progressively harder to erode. Erosion occurs by dislodgement and **entrainment** of aggregates of individual particles (in the form of, for instance, flocs, clumps, or sheets), and the transport capacity of the flow is rarely approached. In this case, using an equilibrium formulation is inappropriate. Instead, transport is typically modeled directly as an erosion rate, for example,

$$M_e = A((\tau/\tau_c)^n - 1), \tau > \tau_c \quad (28)$$

where the erosion rate M_e has units of mass of sediment eroded per unit area of bed per unit time, τ is the bed shear stress, τ_c is the critical stress for erosion of the cohesive sediment, and n is a constant determined by calibration. The constant A , which in this formulation has the same units as M_e , is normally assumed to be a function of only the physicochemical properties of the seabed such as the bed consolidation coefficient, undrained shear strength, bulk density, and mass concentration. Erosion rates may decrease with increasing depth in the bed sediment due to the increase in consolidation. *van Ledden et al.* [2004] provide a good analysis of when a bed is cohesive and when it is not and parameters used to characterize sediment cohesion.

4.1.1. Wave Transport of Suspended Sediment

[69] Few researchers have tried to measure and assess the importance of the wave transport of suspended sediment on intertidal flats. *Christie and Dyer* [1998] showed that the wave transport (which they called the “oscillatory flux”) was about 2 orders of magnitude smaller than the tidal transport

(which they called the “mean flux”) and that the direction of the wave transport was largely random. However, these measurements were from relatively calm weather, when waves were small. *Green et al.* [1997] identified fluctuations in suspended-sediment concentration and current speed at wave frequencies. They found that the wave transport was 10–15% of the tidal transport at around 10 cm above the bed when waves were actively resuspending local bed sediments. The wave transport, which was in the direction of wave advance, added to the tidal transport when the tide was flooding, thus enhancing the total transport. When the tide was ebbing, the total transport was diminished by the wave transport. The wave transport was found to diminish with elevation above the bed, and by about 1 m above the bed it had vanished. Since fine sediments will be suspended higher in the water column than coarse sediments, the waves may have been capable of sorting sediment by grain size.

[70] With respect to the decomposition of the total suspended-sediment transport into tidal and wave components, *Green and MacDonald* [2001] analyzed measurements from an intertidal-flat noncohesive fine-sand bed (mean grain size 150 μm), where waves were generated in the adjacent coastal ocean and entered the estuary by crossing the bar at the estuary mouth. They found that the wave transport of suspended sediment was small compared to the tidal transport, decreased rapidly with elevation above the bed, and on average was directed counter to the tidal current, which they tentatively explained in terms of the orderly ejection from the rippled bed of sediment-laden vortices by the wave-orbital motions. They also found a correlation between a seaward directed forced mean flow [*Shi and Larsen*, 1984] (i.e., opposite to the direction of wave advance, which was from the adjacent coastal ocean) and enhanced suspension under groups of relatively higher waves. This resulted in a persistent offshore suspended-sediment transport at infragravity frequencies (defined as $<1/30$ s) that decreased with elevation above the bed. As before, the changes in the various transport terms with elevation above the bed could lead to sediment sorting by grain size.

4.1.2. Tidal-Current Transport of Suspended Sediment

[71] We focus here on the way waves perturb in regular ways the sediment-transport patterns that otherwise occur during periods of calm weather. Hence, we begin by briefly describing typical calm-weather sediment transport.

[72] On estuarine intertidal flats, tidal-cycle-averaged calm-weather sediment transport is typically directed onshore, due to tidal-current **asymmetry**, **settling lag**, and **scour lag**. Accumulation of fine sediment in the upper reaches of estuaries that arises as a result of settling lag and scour lag was first suggested by H. Postma in a thesis in 1954 and subsequently elaborated by *van Straaten and Kuenen* [1957] and *Postma* [1961]. *Dronkers* [1986] further refined the ideas, and *Pritchard* [2005] elucidated the classic models by analyzing the way different mechanisms, including settling lag, scour lag, and internally generated and externally imposed tidal asymmetries, drive the residual transport of fine sediments in a short tidal embayment.

[73] Settling lag is the period between the time the advecting current reduces to a speed (the “transportation speed”)

at which a sediment particle can no longer be held in suspension and the time it takes for that same particle to finally deposit on the bed. On an intertidal flat where there is a shoreward decrease in tidal current speeds and/or a shoreward decrease in water depth, settling lag will result in a net shoreward transport of sediment. *van Straaten and Kuenen* [1957] provide an excellent description of what is a rather subtle mechanism, which we follow here in order that the effect of waves on the process can be precisely understood. For this explanation, we assume only that tidal currents decrease in a shoreward direction: Currents everywhere across the flat are symmetric in time, variation in water depth across the profile is not considered, and the transportation speed and the “erosion speed” are the same. A particle being transported in suspension shoreward by a flooding tidal current will begin to settle as the water parcel it is moving with decelerates to below the transportation speed. If the particle were to immediately drop to the bed, then the water parcel that it was moving with would carry on up the flat without the particle, eventually stalling at slack water. On its travel back down the intertidal flat on the next ebb tide, the same water parcel would reach the erosion speed at the exact point where the particle was just deposited, and the particle would travel with the water parcel back to where it started from at the beginning of the previous flood tide. Hence, there would be no net particle transport. However, with a settling lag, the particle will deposit shoreward of where it first starts to settle from the water column and, when the original water parcel returns to this spot on the next ebbing tide, it will not yet have reached the erosion speed necessary to entrain the particle. Eventually, another water parcel, which is positioned shoreward of the original water parcel, will reach the erosion speed where the particle is waiting, and it will be transported seaward by this new water parcel but not as far seaward as it began at the start of the previous flood tide. The result will be a net-over-the-tidal-cycle transport of the particle shoreward. Scour lag can also be understood by following the movement of sediment particles and water parcels and also depends on there being a difference between the transportation and erosion speeds. *van Straaten and Kuenen* noted that there is no sharp distinction between the two lag effects and that they are always combined. *Pritchard* [2005] confirmed by mathematical analysis that for fine sediment, “settling lag generally tips the balance in favor of landwards transport,” and he noted a “weak but detectable role of scour lag in enhancing landwards residual transport”, especially when tidal advection is weak.

[74] The ideas of the early Dutch researchers were motivated by the observation that sediments of the Wadden Sea are highly enriched in clay relative to the North Sea source region. *Pejrup* [1988] commented on the role of flocculation, noting that sediment depositing from a flocculated suspension will be eroded as flocs with a structure 1 order higher than the flocs from which deposition took place, which will cause sediment to erode at a higher bed shear stress than that which prevailed during deposition. This will favor sediment accumulation. *Andersen and Pejrup* [2001] observed landward transport of suspended sediment from channels to

adjacent tidal flats during calm weather driven by tidal-current asymmetry, settling lag and scour lag, which resulted in virtually continuous accretion of a microtidal mudflat in the Danish Wadden Sea. *Dyer et al.* [2000] observed net onshore transport of fine sediment during calm weather that was counter to the ebb-dominated tidal currents. They attributed this to lag mechanisms and they pointed out that the result, over time, would be a gradual tide-by-tide movement of sediment landward. *Christie et al.* [1999] presented direct observations of sediment accumulation by scour lag, with less sediment eroded on an ebb tide than was deposited by settling from the water column during the immediately preceding high slack water. They pointed out how the **rheology** of the bed could assist accumulation, with **dewatering** of just-deposited sediments at high slack water increasing the resistance of the bed to erosion on the subsequent ebb tide and consolidation during neap tides of upper flat deposits that are laid down during spring tides. *Christiansen et al.* [2006] also observed a net up-estuary/onshore fine-sediment transport driven by deformation of the tide and by settling and scour lag, aided by flocculation, which caused particle settling speeds to increase near high slack water, thus increasing the sediment settling flux to the bed.

[75] Waves may influence particle settling and therefore net sediment transport, through opposing effects on flocculation, as follows. *Pejrup* [1988] found that increased suspended-sediment concentration under waves enhanced flocculation at high slack water on Danish Wadden Sea intertidal flats, which caused a higher settling flux that in turn reversed ebb-directed calm-weather sediment transport. With the greater accumulation of sediment on the bed, the scour lag was also increased, which further enhanced the net onshore-directed transport. In contrast, *van der Lee* [1998] found that fluid shear—not suspended-sediment concentration—controlled floc size on a tidal flat in the Dollard estuary at the mouth of the Ems River in the Dutch/German Wadden Sea. When waves were present and suspended-sediment concentration was high, there was a reduction in floc size, which they attributed to flocs being broken up by the **wave-induced shear**, and this resulted in a decrease in settling speed, less deposition at high slack water, and loss of suspended sediment to offshore. (The opposite was the case in the channels, where suspended-sediment concentration controlled floc size.)

[76] The direct action of wave-orbital motions and wave-induced bottom turbulence can also have opposing effects on the direction of net transport. Where settling is delayed by the extra wave-induced agitation, the settling lag will be lengthened and the result will be enhancement of the net onshore transport that otherwise would have occurred in the absence of waves [e.g., *Shi and Chen*, 1996]. In contrast, if the extra agitation completely prevents the settling of sediment that otherwise would have occurred at some point in the flooding tide, then the suspended sediment will remain with the “parent” water parcel (as it were), and net onshore transport will be reduced. Many field measurements have demonstrated that onshore-directed calm-weather transport can in fact be reversed by waves [e.g., *Dronkers*, 1986; *de Haas and Eisma*, 1993; *de Jonge and van Beusekom*, 1995;

Ridderinkhof, 1998; *Christie and Dyer*, 1998; *Christie et al.*, 1999; *Dyer et al.*, 2000; *Bassoullet et al.*, 2000; *Janssen-Stelder*, 2000; *Andersen and Pejrup*, 2001], which has usually been attributed to a cancelation of the settling lag effect by the waves preventing the settling of sediment that would otherwise have occurred at high slack water.

[77] *Green and Hancock* [2012] interpreted a situation in which waves enhanced the onshore transport of sediment into a nearby tidal creek as a type of settling lag. Sediments resuspended by waves from an intertidal flat along the margins of the wider estuary into which the tidal creek emptied were transported into the middle reaches of the tidal creek by tidal currents, where they were then deposited and available for relatively slower removal by tidal currents to the upper reaches of the tidal creek, where they were eventually sequestered. *Green and Hancock* interpreted this as waves “cleansing” the wider estuary of fine sediments, since they initiate net landward transport of sediment off the intertidal flats.

[78] Waves may also interact with **baroclinic** processes to affect net sediment transport. For instance, *Ralston and Stacey* [2007] described an intertidal flat where the baroclinic dynamics associated with a salinity front controlled sediment transport, and the calm-weather system was perturbed by wind, waves, and freshwater runoff associated with winter storms. During calm weather, under tidal forcing alone, a narrow salinity front (between salty San Francisco Bay water and fresher runoff from the local watershed) carrying high concentrations of suspended-sediment was advected by flooding currents up the channel and across the flat, but during ebbing tides the front was elongated and suspended-sediment concentrations reduced by tidal dispersion causing spreading of the front. Net sediment transport was weakly onshore due primarily to tidal straining of the salinity front enhancing deposition. During storms, wave resuspension of bed sediments added to the suspended-sediment load, while increased freshwater inputs delivered buoyancy and fine sediment, both of which had a greater effect on the net transport, which was generally directed offshore.

[79] Morphological adjustment depends on the long-term balance between calm-weather tidal forcing and perturbations by episodic storms. For instance, *Kirby et al.* [1993] reported observations of bed elevation over a 22 month period from mudflats in mesotidal Ardmillan Bay (Northern Ireland) which showed seasonal changes. Gale-generated waves were found to cause erosion in winter and spring, and deposition under calmer summer conditions was enhanced by algal binding of the bed sediment. (Refer to *Widdows et al.* [2000] for a description of the way the microphytobenthos influences intertidal-flat sediment erodibility). *Kirby et al.* concluded that episodic wind waves were the main cause of tidal flat instability and noted that this seasonal pattern in accretion and erosion is consistent with previous studies. They also noted that there were no examples from the literature in which a tidal flat was shown to be stable or evolving in one direction only.

[80] Storms, where they result in erosion and offshore transport, can quickly undo the accretion of many tidal cycles. For example, *Christie et al.* [1999] measured accretion of a few millimeters of sediment per tidal cycle by tidal currents in calm weather, against a single storm that produced several centimeters of erosion. However, they also observed rapid accumulation of sediment following storm erosion, with the result that the energetic events tended to cancel, producing seasonal bed-level changes of just a few millimeters. *de Haas and Eisma* [1993] distinguished between fair weather (onshore transport by tidal current of sediments resuspended in the development of a turbulent front during the early flood when the flats are submerged), windy weather (sediment kept in suspension by waves), and storms (erosion of intertidal flats and large loads of suspended sediment transported seaward). From this they deduced that there are seasonal variations in sediment transport. This is supported by the sedimentology, which shows only a small fraction of the summer deposition left after the winter season, resulting in a small annual accumulation of fine sediment. *Dyer et al.* [2000] also concluded that there is a fine balance between seasonal accretion and erosion, with the net result depending on the relative durations of storms and calms, and they also noted that other seasonal cycles may interact with the waves and currents. Specifically, they showed that wave erosion of the intertidal flats causes the mud content of the surface sediments to reduce, which in turn decreases algal diatom cover and reduces the erosion threshold. In contrast, mud content of the bed sediment increases during calms, which could increase diatom cover and make them harder to erode. *Andersen and Pejrup* [2001] also noted that it is not only waves that vary seasonally, pointing out that seasonal variations in temperature and solar radiation play a role through biological effects on both bed stabilization and sediment-particle flocculation.

4.2. Bed Load Transport

[81] Very little work has been done on **bed load** sediment transport by waves in estuaries.

[82] *Green and MacDonald* [2001] estimated the transport of sediment carried as bed load by waves and currents in combination. For this, they adapted *Bailard’s* [1981] “quasi-steady” formulation, in which there is a direct relationship between bed load transport and flow velocity at each phase in the wave cycle, with no phase lag. *Green and MacDonald* estimated the magnitude of the bed load sediment transport Q_b from burst velocity measurements as

$$Q_b = \left\{ \left[\left(\frac{\rho_s C_d \varepsilon_b}{g \tan \phi} \right) \frac{1}{B} \int_0^B V^2(t) u(t) dt \right]^2 + \left[\left(\frac{\rho_s C_d \varepsilon_b}{g \tan \phi} \right) \frac{1}{B} \int_0^B V^2(t) v(t) dt \right]^2 \right\}^{1/2} \quad (29)$$

where C_d is the drag coefficient appropriate to the level of the velocity measurements, ε_b is the bed load efficiency, ϕ is the internal angle of friction, B is the burst duration, u is the east-erly component of V , and v is the northerly component of V .

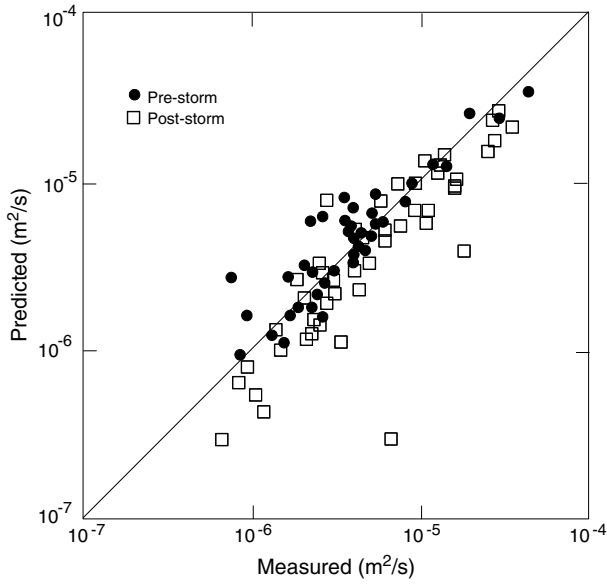


Figure 9. Comparison of volumetric bed load transport rate (volume of sediment per unit time and unit width) measured using a dune-tracking technique and predicted using an adaptation of *Ribberink's* [1998] formula. Redrawn from *Hoekstra et al.* [2004] with permission from Elsevier.

ϕ_b , the direction of bed load transport, was estimated from the velocity data as

$$\phi_b = \tan^{-1} \left[\frac{\frac{1}{B} \int_0^B V^2(t) u(t) dt}{\frac{1}{B} \int_0^B V^2(t) v(t) dt} \right] \quad (30)$$

[83] Bed load transport so estimated was directed up estuary on both flooding and ebbing tides due to the wave **skewness**: During floods, the tidal current and the waves added together to drive bed load transport up the estuary; during ebbs, the waves and currents acted against each other, but increasing wave skewness toward low tide resulted in a net-over-the-ebb up-estuary bed load transport anyway.

[84] Whereas *Green and MacDonald* estimated bed load from velocity data, *Hoekstra et al.* [2004] applied a dune-tracking technique to estimate bed load sediment transport on Spratt Sand, which is an intertidal shoal located at the mouth of Teignmouth, Devon (UK) and which is composed of a thin veneer (0.10–0.30 m) of loosely packed sand (250–300 μm median grainsize) and gravel (1.1 mm) on top of a rocky substratum. They found that bed load transport rates were a factor of 2 greater under extreme wave conditions compared to average wave conditions and that tide-driven bed load transport, although consistent, was significantly smaller than bed load transport under combined waves and currents. *Hoekstra et al.* compared their estimates of bed load with predictions by *Ribberink's* [1998] semiempirical model for bed load under current, wave, and combined wave-current flows, which they formulated as follows:

$$\overrightarrow{\langle \Phi_{b(t)} \rangle} = m \langle (|\Theta'_{t,wc}(t)| - \theta'_{crit})^p \frac{\overrightarrow{\Theta'_t(t)}}{|\Theta'_t(t)|} \rangle \quad (31)$$

[85] Here Φ_b is the dimensionless bed load transport rate, $\Theta'_{t,wc}$ is the dimensionless skin friction due to the combined wave-current flow, the brackets $\langle \rangle$ denote a time average, the arrow represents a vector quantity, and m and p are empirical constants (taken to be 11 and 1.65, respectively). *Hoekstra et al.* found good agreement between observations and model predictions (Figure 9), even though the model was formulated for quite different conditions (sheet flow over a flat bed) and had to be adapted somewhat for the dunes that were present at Spratt Sand. For the combination of small currents and low-to-moderate waves, measured and predicted bed load transport rates differed by 10–20%, and the maximum discrepancy occurred under the most energetic waves, when the model underestimated the measurements by as much as one half. The *Ribberink* model appeared to perform better prior to storms than after storms. *Hoekstra et al.* also noted that suspended-sediment concentration was largest when wave-orbital speeds at the bed exceeded 70 cm/s but that strong tidal currents of up to 1 m/s hardly caused any suspension. They attributed this to “hiding” of the more mobile sand grains by the less mobile gravel grains, which were disrupted by the wave action, resulting in both bed load and suspended-load transport.

[86] Also concerning bed load sediment transport, *Quaresma et al.* [2007] linked the formation of depositional ridges in salt marshes to landward transport by locally generated wind waves of shells as bed load across intertidal flats in Southampton Water (UK). Dyed shells, placed at different locations (lower mudflat, upper mudflat, and on a depositional ridge in a salt marsh), were found to be transported mainly by wave action with tidal currents having virtually no effect, and the direction of transport was uniformly landward, which was opposite to the direction of net suspended-sediment transport.

4.3. Fluid Mud

[87] Focusing just on shear stresses may underestimate the importance of waves to sediment dynamics by overlooking the potential of waves to fluidize muddy beds, which can initiate various forms of mud transport.

[88] *McAnally et al.* [2007] defined fluid mud as “a high concentration aqueous suspension of fine-grained sediment in which settling is substantially hindered by the proximity of sediment grains and flocs, but which has not formed an interconnected matrix of bonds strong enough to eliminate the potential for mobility.” *Mehta* [1991] noted the fundamental distinction between fluid mud, which is a fluid-supported particle assemblage with an effective normal stress of practically zero, and a cohesive-sediment bed, which has dewatered sufficiently to form a fully particle-supported assemblage. *Winterwerp* [1999] differentiated between highly concentrated mud suspensions, which have particle concentrations from a few hundreds of milligrams per liter to a few grams per liter, and fluid mud, which may have concentrations exceeding hundreds of grams per liter. A sediment-particle concentration of 10 g/L is commonly accepted as the lower limit defining a fluid mud [*Kineke et al.*, 1996].

Fluid mud layers are typically clearly delineated at the top by a **lutocline**, but the lower interface with the bed is harder to define since that interface may not correspond with the zero-velocity plane [Ross and Mehta, 1989]. Fluid mud viscosity ranges from 2 to 4 orders of magnitude greater than that of water [Rodriguez and Mehta, 1998], which has a profound effect on the rheology and therefore the dynamics of the mud itself and on the dynamics of waves traveling overhead [e.g., Mathew et al., 1995; Calliari et al., 2001; Sheremet et al., 2011].

4.3.1. Formation and Transport of Fluid Mud

[89] It is useful to distinguish between the formation and the transport of fluid mud.

[90] Following McAnally et al. [2007], there are two classes of formative process. The first class lumps those processes that act to accumulate a large mass of fine sediment at a rate that exceeds the rate of dewatering of the suspension. The processes in this class include the settling of sediment from above in the water column, which may initially be enhanced by particle aggregation but ultimately hindered as sediment concentrations continue to increase [e.g., Winterwerp, 2002] and the convergence or deceleration of sediment-transporting flows. A sufficient supply of fine sediment is always necessary for fluid mud to form, and in some cases it would appear that a very large supply of fine sediment is all that is needed. For example, banks of fluid mud on the northeast coast of South America are formed by seasonal variations in a massive supply of fine sediment from large river systems [Anthony et al., 2010]. The second way fluid mud can form is by fluidization of a cohesive-sediment deposit, which occurs when aggregates become separated, leading to the sediment becoming fluid supported instead of grain supported. The dynamic pressure associated with **surface gravity waves** can cause fluidization to occur by generating a gradient in excess **pore water pressure** which in turn drives an upward **pore water** flow that exerts a drag force that may break aggregate bonds and/or exceed the effective weight of the sediment overburden. (See Li and Mehta [1997], for a detailed description of mud fluidization by water waves.) This process requires that the bed is not rigid and has a low permeability; it does not require particularly energetic waves, since the buildup of pore water pressure is a gradual process, occurring over many wave cycles [Maa and Mehta, 1987]. Mehta [1996] noted that mud can remain fluid supported for as long as the waves persist but that the particle-supported matrix, with a measurable resistance to shear, rapidly reestablishes when the waves cease. If the bed is sufficiently permeable, excess pore water pressure cannot be sustained; the permeability of a bed of noncohesive sediment is typically sufficient to dissipate pore water pressures before they become critical.

[91] Once formed (by whatever mechanism), fluid mud may be transported in a number of ways, among them are the following: by gravity acting on fluid mud resting on a sloping seabed, by streaming under progressively damped, nonbreaking waves [Rodriguez and Mehta, 1998], and by vertical entrainment into an overlying transporting flow. Shi et al. [1997], following Mehta et al. [1989], Scarlatos and Mehta [1990], and Mehta and Srinivas [1993], emphasized

the distinction between fluid mud entrainment, which they called “reentrainment,” and resuspension of a cohesive mud bed, the former being controlled by the stability of the lutocline that bounds the top surface of the fluid mud layer and the latter being characterized by dislodgement and entrainment of surface aggregates by shear stresses. Reentrainment may occur across a range of scales, including “eddy stripping” [McAnally et al., 2007], continuous entrainment when boundary-layer turbulence is sufficient to mix the lutocline, and entrainment of a fluid mud layer en masse following a failure of the layer along the lower internal boundary caused by fluid drag across the top of the lutocline.

4.3.2. Fluid Mud in Estuarine Basins and Channels

[92] Pools of fluid mud have been observed in deep basins and channels of estuaries, where it is known to form as sediment-transporting flows converge, it is quiescent enough for settling aided by flocculation to clear the water column of fine suspended sediment, and there is sufficient sediment accommodation space. For example, Li and Zhang [1998] inferred fluid mud formation in the Chiangjiang estuary as a result of settling of suspended sediment in a turbidity maximum that in turn was formed by **salinity intrusion** and vertical **gravitational circulation**. Uncles et al. [2006] described fluid mud formation associated with an estuarine turbidity maximum (ETM) in the macrotidal Humber River estuary (UK). The accumulation of fluid mud was attributed to the combination of longitudinal advection of suspended sediment by a pronounced tidal asymmetry, estuarine gravitational circulation, and sediment settling around slack water, the latter being aided by flocculation that enhanced the settling of very fine particulate matter. Wolanski et al. [1995] described the formation of fluid mud in the macrotidal Fly River estuary (New Guinea) that was also associated with an ETM. The ETM in turn was caused by convergence of sediment-laden flows driven by the mean baroclinic circulation and tidal pumping by asymmetric tidal currents. Kirby and Parker [1983] observed sediment settling under decelerating tidal flows in the macrotidal Severn estuary (UK) forming a lutocline that continued to settle toward slack water, which in turn formed fluid mud in deep channels that was 2–3 m thick. During spring tides, the fluid mud so formed was dispersed under accelerating tidal flows after slack water, but during neaps the lutocline remained intact, and fluid mud was dragged back and forth en masse by tidal currents until springs recurred, at which time the lutocline would begin to break up. In contrast to the in situ formation of fluid mud observed in the Severn, Kirby [1986] described fluid mud in the mesotidal Rhine estuary (Germany) that is advected there from the North Sea, where it is entrained by storm waves. Once inside the estuary, the fluid mud “stagnated.” Wolanski et al. [1988] described how sediment-induced stratification of the bottom boundary layer damped vertical mixing, which assisted the development of a lutocline during ebb tides in the macrotidal South Alligator River estuary (Australia), which in turn contributed to the formation of mud banks. Nichols [1985] described pools and blankets of fluid mud greater than 20 cm thick in the James River estuary (Chesapeake Bay) associated with a

turbidity maximum near the inner limit of salt intrusion and noted that any behavior that increases sediment mass flux to the bed, resists erosion, and then deters consolidation will promote the accumulation of fluid mud, even in the presence of fast tidal currents. *Nichols* cited as examples of such behavior the stratification of interfacial fluid, pore water, and suspended sediment, which inhibits upward mixing and diffusive exchange, the **pseudoplastic** properties of fluid mud, flocculation, and change of settling speed as a function of concentration and extent of aggregation. *Nichols* further noted that fluid mud acts as a reservoir of sediment to any overlying transporting layer, as well as stabilizing underlying deposits.

[93] Wave erosion of sediment deposits in tidal rivers and around the landward margins of the estuary can add to the pool of mobile fine sediment in the estuary, including that held within an estuarine turbidity maximum and deposits of fluid mud. For instance, *Couperthwaite et al.* [1998] showed that erosion of the upper bank at Burringham on the River Trent (UK), a tidal river at the head of the Humber estuary system, is controlled primarily by waves, which destabilize sediment that is deposited during spring tides when sediment supply to the margins is greatest. On the lower bank, the lunar-cycle variation in the tidal-current bed shear stress controlled deposition. Erosion was due to the waves, which produce erosive “bench forms,” and by block failures (or cliffing), which occurs as negative pore water pressure rises in the plane of the vertical bench following the recession of the tide [Allen, 1984]. Erosion was modulated by consolidation of the bank through surface drying and by microbial stabilization. *Mitchell et al.* [2003] largely confirmed *Couperthwaite et al.*'s results. Their observations, which were made at Blacktoft on the River Ouse, which is also a tidal river at the head of the Humber estuary, showed that net deposition occurs under a high supply of sediment and low wind speed and erosion occurs under high wind speed and low sediment supply, thus confirming the view that deposition is linked to sediment availability and erosion to waves. *Kitheka et al.* [2005] attributed the formation in the Tana estuary (Kenya) of a low-tide turbidity maximum during spring tides partially to wave resuspension of bed sediments that subsequently became trapped at the toe of a **salt wedge** and partially to sediment supplied by the river. The turbidity maximum was further enhanced by tidal pumping and flocculation that in turn was induced by changes in salinity.

4.3.3. Fluid Mud on Intertidal Flats

[94] In addition to the pools of fluid mud found in deep basins and channels of estuaries, fluid mud has also been found draping (loosely covering) macrotidal intertidal flats.

[95] For example, *Christie et al.* [1999] found fluid mud accumulating at high slack water springs on the macrotidal Skeffling intertidal flats (Humber River estuary, UK) which they attributed to a large-scale cycling of mud between deep-water channels, where fluid mud is thought to accumulate and remain stationary during neap tides, and adjacent intertidal flats. The transfer of mud from stores in the deep channels to the flats, they reasoned, is triggered by tidal currents exceeding a certain threshold at some point in the transition from neap to spring tides. This results in a fortnightly

variation in the supply of mud to the intertidal flats and produces significant accretion of mud during calm spring tides. *Christie et al.* also observed the formation of fluid mud on the Skeffling intertidal flats at high slack water by the settling of fine sediment eroded from the bed by waves during the preceding flooding phase of the tide. In one instance, approximately 6 cm of hard, overconsolidated bed sediment was eroded from the bed by waves in the first 2 h of a flooding tide. The erosion rate subsequently dropped as, on the one hand, the water depth increased and waves became increasingly less able to penetrate to the bed, and on the other hand, deeper layers of bed sediment with an increasingly high critical bed shear stress were exposed. Based on measurements of in situ particle settling rates, *Christie et al.* inferred that settling of the suspended sediment at high slack water could produce a fluid mud layer, which was supported by observations of 3 to 4 cm of deposition at slack water. However, the fluid mud so formed was rapidly reentrained by the same waves on the next ebbing tide and exported to and dispersed within the deep interior of the estuary. In one case, this resulted in a per-tidal-cycle offshore transport of mud from the intertidal flats that was equivalent to 3% of the suspended sediment transported in and out of the estuary during a typical spring tide. *Christie et al.* [1999] pointed out that the offshore transport of fine sediments that are either resuspended from an intertidal cohesive bed by waves or reentrained from a fluid mud layer by waves will add to the pool of mobile fine sediment in the deeper reaches of the estuary.

[96] *Bassoullet et al.* [2000] described fluid mud on the Brouage upper intertidal flats in the macrotidal Bai de Marennes-Oleron (France), which they attributed to spring-tidal currents mobilizing a bay-wide pool of fine sediment, resulting in a net onshore sediment flux and deposition of mud on the upper intertidal flats. Waves were “easily” able to remove fluid mud so emplaced when it had not been in place for a sufficient time to begin dewatering and consolidation. *Bassoullet et al.* noted that tidal currents control the subsequent transport and redistribution of the muds that are resuspended or reentrained by waves. Their data showed significant increases in suspended-sediment concentration in channels during periods of wave activity, which will have added to the larger pool of fine sediments in the estuary. *Gouleau et al.* [2000] used **radioisotope dating** to confirm that fluid mud is a temporary feature of the Brouage mudflats.

4.3.4. Effect of Bed Fluidization on Fluid Mud Formation and Bed Erodibility

[97] There does not appear to be any evidence for wave fluidization of intertidal-flat bed sediments causing the formation of fluid mud in situ. Although large waves are not necessary to cause a mud bed to fluidize, sufficient time is required for the pore water pressure to build to the point of inducing failure of the sediment matrix. Furthermore, any fluid-supported state that does develop will quickly collapse once the waves cease. In the case of locally generated wind waves on estuarine intertidal flats, for which the ratio of wavelength to water depth is small at high tide, wave-driven pressure fluctuations will penetrate down to the bed

for only a fraction of the tidal cycle. Approaching low tide, the shear stress exerted on the bed by the waves may cause bed-sediment resuspension, and of course the intertidal-flat bed will emerge at some time before low tide, further limiting the interval when fluidization may occur.

[98] The same is not necessarily the case, however, for subtidal beds, where there is evidence for wave fluidization, resulting in changes to bed erodibility. For instance, *Sanford* [1994] showed data from the Upper Chesapeake Bay that suggested that locally generated wind waves can increase bed erodibility considerably in the short term, which was tentatively attributed to partial fluidization of the upper bed sediments by the waves, which changes the consolidation state. *Wolanski et al.* [1995] inferred wave fluidization of a muddy sand subtidal seabed (5–10 m depth) in the Fly River estuary (New Guinea), from the observation that the erosion rate was strongly dependent on the wind speed. In this case, the erosion rate was formulated to account for the limit to erosion imposed by the increasing compaction of sediment with depth in the seabed. *Wolanski et al.* interpreted a 4 times increase in erosion rate under 15 m/s trade winds compared to during calm weather as indicative of disruption of the bed fabric by waves (i.e., wave fluidization of the bed), pointing out that if the waves only influenced erosion by increasing the bed shear stress, then the critical current speed for initiation of sediment resuspension would have been smaller with the waves present, which was not the case.

[99] *Wolanski and Spagnol* [2003] also inferred fluidization of a muddy sand seabed in 5 m water depth in King Sound (Western Australia) by waves that had period 3–3.5 s and that were 1–1.5 m high. Applying similar reasoning to that applied to the Fly River data, the calibration constant A in the cohesive-sediment erosion rate (equation (28)) was found to vary strongly with wave height. As pointed out above, A is normally assumed to be a function only of the physicochemical properties of the seabed, but the King Sound data showed that it was 10 times larger on ebb tides, when the wave height was 1.5 m, compared to on flood tides when the wave height was 1.0 m, and τ was formulated to include only the stress due to the tidal current. *Wolanski and Spagnol* inferred this result as indicating that waves fluidize the bed through a buildup of pore water pressure which then “adds to” the erosion produced by the excess bed shear stress. *Wolanski and Spagnol* pointed out that no fluid mud layers were actually observed in King Sound, noting that as soon as bed sediment is fluidized, it is reentrained (in the language of this review) and mixed upward through the water column by the tidal current.

[100] Building on these observations and noting that bed fluidization should always occur under waves, even when the waves are very small, *Lambrechts et al.* [2010] recently proposed a way for accounting for the effect of the wave-induced pore water pressure on the erosion rate. The M_c was explicitly partitioned into a component E_1 due to the buildup of wave-induced pore water pressure and a component E_2 that is of the same form as equation (28). Then, following the earlier work by *Wolanski* and others

[*Rodriguez and Mehta*, 2000; *Foda and Huang*, 2001], E_1 was related to a high power of the significant wave height H_s by

$$E_1 = \alpha_1 H_s^3 F_1(\omega, h) \quad (32)$$

where α_1 is an empirical constant the value of which depends only on the physicochemical properties of the seabed sediment and the function F_1 is given by

$$F_1 = \exp(-0.905\omega^2 h/g - 0.027) \quad (33)$$

following *Kuo and Chiu* [1994] and *Tsai et al.* [2005]. *Lambrechts et al.* used this formulation to successfully reproduce measurements of suspended-sediment concentration in Cleveland Bay (Australia) under a range of wave conditions. This approach, to explicitly account for the effect of waves on the erosion rate, merits further attention.

5. EXPLORATORY MODELS

[101] Exploratory models [in the sense of *Murray*, 2003] have yielded some deep insights into the behavior of waves on intertidal flats. For example, *le Hir et al.*'s [2000] reasonably simple formulation of wave dissipation reveals how spatial and temporal patterns in wave-induced bed shear stress evolve and interact, and this can provide a powerful framework within which to interpret measurements of resuspension and sediment transport.

[102] Exploratory models have also been used to develop insight into morphological evolution, which depends on the divergence of sediment fluxes. A particularly fruitful area of morphodynamic modeling has been stimulated by observations of intertidal-flat profiles and hypsometry, the latter being the relationship between elevation and cumulative intertidal-flat area.

[103] *Friedrichs and Aubrey* [1996] developed an analytical model to explore and explain observations of hypsometry. *Friedrichs and Aubrey*'s model was based on the assumption that the equilibrium shape of a tidal flat is associated with a uniform spatial distribution of bed shear stress, which they reduced to a uniform distribution of maximum velocity by assuming a constant drag coefficient. They acknowledged that this was a simplification of the more correct formulation which would be in terms of zero divergence of the net sediment transport. *Friedrichs and Aubrey*'s key discovery was that neither the maximum tidal-current bed shear stress nor the maximum wave-generated bed shear stress can be uniformly distributed across a tidal flat that slopes linearly away from a straight shoreline, and therefore, the linear flat is not stable. Instead, when the ratio of tidal to wave activity is high (tidal currents dominant) the equilibrium hypsometry is convex, and when the ratio of tidal to wave activity is low (waves dominant) the equilibrium hypsometry is concave. Furthermore, they were able to provide insight on the physical controls on intertidal-flat geometry. For example, in the absence of waves, the equilibrium length of an intertidal flat (in the direction of the maximum tidal-current velocity) at the base of a straight shoreline was found to be directly proportional to the tidal period

and the characteristic tidal-current speed, but on a wave-dominated flat the equilibrium length was found to be inversely proportional to offshore wave height and directly proportional to the square of the tide range. *Friedrichs and Aubrey* showed how consideration of these scales helps explain the association of small tidal ranges with concave hypsometry and large tidal ranges with convex hypsometry. Furthermore, if waves dominate over currents in the upper part of the intertidal flat but currents dominate over waves in the midpart of the flat, the observed profile shape might carry a signature of both waves and tides.

[104] *Roberts et al.* [2000] tackled the same problem but assumed that equilibrium corresponds to “zero net sediment transport at each point along the profile” over a chosen time period (either a tidal cycle or a spring-neap cycle). (For a detailed derivation of the analytical solution of this problem, the reader should refer to Appendix C of *de Swart and Zimmerman* [2009]). For the case of cross-shore tidal currents only, mass and momentum conservation were stepped through time and coupled to a sediment-transport equation, leading to changes in bed level. Imposing sinusoidal tides yielded profiles that were qualitatively similar to the ones obtained by *Friedrichs and Aubrey* [1996], even though the resulting bed shear stress distribution was not spatially uniform. Since sediment dynamics are included in the model of *Roberts et al.*, it is possible to use the model to assess the role of various processes that might affect profile shape. Limiting bed erodibility (e.g., as a result of **biostabilization**) and providing a large sediment supply both increase deposition and result in a flatter profile, while a steeper profile results from increased erodibility. The effect of waves was included by introducing a bed shear stress in the form of equation (15). Under constant offshore wave forcing, profiles became concave and were similar to the ones obtained by *Friedrichs and Aubrey* [1996]. Model results were in agreement with the observations of mudflat geometry at Skeffling in the Humber estuary, although any comparison of the upper part of the flats should account for the limited validity of the model assumptions in very shallow water. Also, upper areas are usually dominated by vegetation which, with feedbacks with hydrodynamics and sediment transport, dominates sedimentary processes.

[105] *Fagherazzi et al.* [2006] examined the implications for estuarine bathymetry of the nonmonotonic relationship between wave-induced bed shear stress and water depth, which was explored in some detail in section 2 of this review. Their analysis applied specifically to the Venice Lagoon but was claimed to be generally valid for microtidal and mesotidal environments away from tidal channels, where sediment resuspension is largely due to locally generated wind waves, not tidal currents or longer-period waves propagating from offshore. The time rate of change of the vertical elevation of the tidal flat was related to the balance between an annual-average deposition rate, which was imposed, and an annual-average erosion rate, which was related to τ_w and a critical bed shear stress for initiation of sediment motion. Comparing the erosion rate that exactly balances a deposition rate that is constant across the flat against the typical cross-flat

distribution of τ_w , which peaks at an intermediate water depth, was shown to lead to a bimodal distribution of stable bottom elevations. These are the intertidal flat and the salt marsh. Other elevations were found to be unstable, tending toward one or other of the stable elevations. The elevation $z_{\tau_w, \max}$ corresponding to the maximum in τ_w is a key control, as it represents the boundary between stable and unstable elevations. *Fagherazzi et al.* showed that elevations less than $z_{\tau_w, \max}$ (that is, where the water is deeper than the water depth corresponding to the maximum in τ_w) are all the possible equilibrium elevations that a tidal flat can attain as a function of different deposition rates. Conversely, the elevations greater than $z_{\tau_w, \max}$ (water shallower than the water depth corresponding to the maximum in τ_w) are all unstable, being areas that are in transition to marshes or vice versa. Where the deposition rate decreases with decreasing water depth (which does occur in marshes because of the decrease in inundation time but which may not be the case on open intertidal flats), the boundary between unstable and stable elevations shifts to a higher elevation (water shallower than the water depth corresponding to the maximum in τ_w) than that in the constant-deposition case. However, the boundary is still keyed directly to $z_{\tau_w, \max}$, emphasizing the importance of the wave-induced bed shear stress.

[106] Within the Venice Lagoon, it is evident that wind waves play an erosive role, and the same applies to other more recent studies [e.g., *Marani et al.*, 2010; see also *Fagherazzi et al.*, 2012] in which wind waves play a critical role in a balance between tidal landforms and biota (microphytobenthos and marsh **halophytic vegetation**), resulting in multiple stable states. More studies continue to address the role of wave erosion of salt marsh boundaries [e.g., *Mariotti and Fagherazzi*, 2013a].

[107] *Wang and Temmerman* [2013] analyzed records from the macrotidal current-dominated Western Scheldt estuary (Netherlands) and verified the hypothesis by *Fagherazzi et al.* [2006], subsequently elaborated upon by *Defina et al.* [2007], that bare intertidal flats and vegetated marshes are the only two alternative stable states in intertidal areas of estuaries, deltas, and coastal embayments and that shifts between the two states, when they occur, are rapid.

[108] *Friedrichs* [2011] noted that tidal-flat morphology typically approximates a dynamic equilibrium that lies somewhere between the purely tide-dominated and purely wave-dominated extremes, when averaged over annual and longer timescales. Around that dynamic equilibrium, tidal-flat profiles are attracted to one or the other of the extremes by different forcings. For example, as far as the balance between waves and tides go, a more convex profile is favored by increased tidal range, decreased wave height, forcing by a faster-rising tide, and/or external forcing by a tide with an extended period around high water. A more concave profile is favored by decreased tidal range, increased wave height, forcing by a faster-falling tide, and/or external forcing by a tide with a shortened period around high water. The reader is referred to *Friedrichs* [2011] for a comprehensive review of the morphological adjustment of tidal flats to various forcings, including a summary conceptual diagram, which is reproduced here as Figure 10.

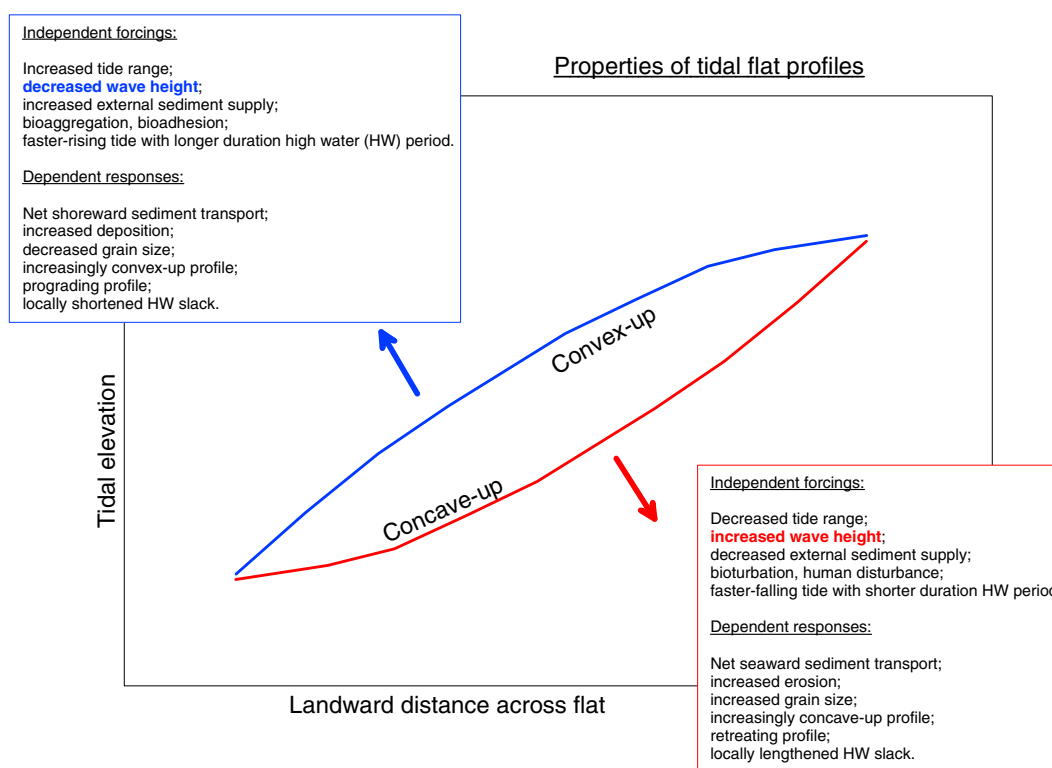


Figure 10. Conceptual diagram of the response of tidal-flat shape and properties to a variety of independent forcings, including waves (highlighted). Redrawn from *Friedrichs* [2011] with permission from Elsevier.

[109] *Mariotti and Fagherazzi* [2013c] showed that even though channel sediment dynamics are driven by currents and intertidal-flat sediment dynamics are driven by waves, as has been shown by a wide range of field measurements, channel-flat morphology is controlled by interaction between the two. Furthermore, the system dynamics and geometry depend most importantly on wind speed (meaning wave height) and, in fact, equilibrium intertidal flats can only exist when there are waves.

[110] To demonstrate this, *Mariotti and Fagherazzi* simulated the tidal dispersion between two reservoirs of variable volume—one representing channels and the other flats—arising from a symmetrical tidal exchange flow and a spatial gradient in suspended-sediment concentration. This was viewed as an advance over previous channel models, which have generally used a one-dimensional schematization with tidal flats as water storage that have no role in the momentum balance, and previous intertidal-flat models, which have either used transects parallel to the main flow direction with a sediment boundary condition representing inputs from a channel to the adjacent flat or else a flat surface characterized by a single elevation.

[111] A key feature of *Mariotti and Fagherazzi's* “two-point” dynamic model is the use of a reference concentration in each reservoir, which establishes the concentration gradients. The reference concentration in each reservoir is determined by the bed shear stress associated with currents and with waves, which are computed separately from each other, and which are based on characteristic or “reference” conditions, including the wind speed, fetch, and depth for the wave-generated stress.

[112] With no waves present, there is only one stable equilibrium point in the phase-space plot of channel versus intertidal-flat depth, which corresponds to a channel with surrounding flats at the mean-high-water elevation. This resembles a creek-marsh morphology. A second equilibrium point, corresponding to an unchannelized flat, was not stable. For low wind speeds, in the so-called current-dominated regime, the equilibria were the same as those for the current-only condition. For intermediate-strength winds, in the so-called mixed regime, a new stable equilibrium arises, which is characterized by a channel flanked by intertidal flats close to the elevation of mean low water, and the channel and the intertidal flat mutually readjust their respective elevations in response to changes in control parameters. The equilibrium arises from a dynamically balanced sediment exchange between the channel, where sediment resuspension is controlled by currents, and the flat, where the control is by waves. “Dynamic” in this sense means that nonzero instantaneous sediment fluxes average to zero over certain timescales such as a tidal cycle or the time between formative wave events. The model predicted that the tidal flat deepens with an increase in wave intensity and a decrease in sediment concentration at the sea boundary, which is consistent with previous cross-flat and one-point models. In the strongly wave-dominated regime, there is only one stable equilibrium, in which large waves associated with strong winds suppress channel formation. Unlike in the mixed regime, where there is a balance between waves and currents, in the strongly wave-dominated regime waves alone control tidal-flat elevation. Furthermore, channel depth is indirectly controlled by

the waves through the influence of tidal-flat elevation on channel hydrodynamics.

6. FUTURE DIRECTIONS

[113] There is ample experimental evidence to conclude that waves typically erode estuarine intertidal flats, which can be thought of as otherwise accreting in the absence of waves. The evidence supporting the view of waves as agents of erosion includes measurements of sediment flux, typically at the event timescale, and measurements of bed level at event, seasonal, and longer timescales. Although net offshore transport of suspended sediments during storms is often ascribed to the action of waves canceling the settling lag effect, this cannot be a complete explanation. There are other factors to consider. For one thing, intertidal flats are connected to channel networks that convey water and suspended sediment at low tide when intertidal flats are uncovered. For instance, *Green et al.* [2000] found the distinctive features of an intertidal flat wave-driven turbid fringe transiting a deep channel in the middle of Manukau Harbour (New Zealand), which suggests widespread dispersal of resuspended sediments. *Dyer et al.* [2000] noted that sediment resuspended by waves from intertidal flats and kept in suspension over high slack water becomes concentrated in the channel network and is dispersed widely through the basin by ebb-dominated tidal currents. *Christie et al.* [1999] also observed net offshore sediment transport from an intertidal flat, even though the tidal currents there were flood dominated. They noted that sediment eroded from the intertidal flats by waves may remain in suspension during most of the ebb tide and thus be transported a long distance in a seaward direction. *Ridderinkhof* [1998] viewed the higher concentrations of suspended sediment in the Ems-Dollard basin due to waves as causing a net seaward diffusive flux of sediment, which balances shoreward lag-driven transport.

[114] The same winds that generate waves may also generate currents that can advect suspended sediment. For instance, *de Haas and Eisma* [1993] found that sediments resuspended by high waves were transported seaward by an ebb flow that was enhanced by the relaxation of a storm surge on the ebbing tide. *le Hir et al.* [2000] noted that the local tidal flows as well as inundation times may be changed by storm surge and that the entrainment by the wind of surface waters was likely to induce return flows in deeper waters. *Ridderinkhof et al.* [2000] found that the net transport of suspended sediments on the Ems-Dollard intertidal flats was variable and strongly dependent on wind direction. Specifically, they found that westerly winds could increase transport “drastically” but the direction could be either landward or seaward, which led them to suggest that the direction of net transport can be both seaward and landward, depending on where erodible sediments have been previously deposited. They concluded that wind events “mainly cause an internal redistribution of fine-grained sediments within the basin.” *Nowacki and Ogston* [2012] found significant increases in mean current speed on an intertidal flat and in adjacent channels when it was windy compared to when it

was calm and also that the wind steered the flow. Furthermore, the wind modified the intensity of a velocity pulse in a channel that was related to the movement of water onto and off from the tidal flats. The intensity of the ebb pulse was reduced significantly by wind speed but weakly enhanced on the flood, which resulted in an increased net upstream transport of suspended sediment by a factor of about 3 compared to calm weather, which they noted contrasted to the mainly European data that show wind events enhancing ebb transport. They account for the difference in terms of the local morphology and alignment of the channels, noting that a study by *Mariotti and Fagherazzi* [2011], also on tidal flats in Willapa Bay, found channels to be ebb-dominated.

[115] However, our knowledge is largely empirical. To support this view, we note that much of the literature cited in this review—with some notable exceptions—reports only observations, usually in the form of **time series**. For instance, although the wave-driven turbid fringe would appear to be a ubiquitous feature of estuaries in windy weather, we have no real understanding of its dynamics. This is a significant deficiency, since within the turbid fringe SSC is higher than at any other location in the water body straddling the intertidal flat (by definition), and sediment fluxes within the turbid fringe may be comparable to sediment fluxes at other stages of the tide. Several factors are in play: The turbid fringe occupies water depths where wave-orbital motions are capable of penetrating down to the bed; being at the extreme end of the fetch, whitecapping may be a factor in mixing of turbulent energy down from the surface; a surfzone may occupy or intersect the turbid fringe; and, when the turbid fringe is at the leading edge of a flooding tide, it is encountering sediment that has been exposed to the air for a period of time, which may have altered its properties vis-à-vis erosion. Due to the difficulties of making measurements in very shallow water, many published data sets are truncated and capture only a part of or miss altogether the turbid fringe. To explore the dynamics of the turbid fringe in particular and the leading edge of the water column in general, measurements in very shallow water are required. Experiments may be conceived to follow the turbid fringe as it transits the intertidal flat in order to maximize the data length and to observe how the fringe evolves over the tidal cycle. *le Hir et al.* [2000] pointed out that assessing the contribution of different forcings to the generation of bed shear stress in shallow water in estuaries is complicated, because of bed irregularities due to drainage, drying and swelling of muddy beds, **bioturbation**, and emergent vegetation. Furthermore, classical laws that can be used to calculate bed shear stress are questionable in very shallow water. Hence, new, more appropriate models for interpreting field data from very shallow water may be required.

[116] A significant measurement problem is that of separating measured suspended-sediment concentration into that part that is due to resuspension of the local bed sediment and that part that has been resuspended elsewhere and advected by currents to the measurement site. Where it is not possible to make this separation it is also not possible to analyze the effect of the local shear stresses on the bed sediment. This problem appears to be exacerbated on estuarine

intertidal flats compared to, say, open-coast sandy beaches, because intertidal flats are typically composed of relatively finer sediment which has a smaller settling speed and which therefore will stay in suspension for longer periods and be advected further. Where sand resuspension by waves in estuaries has been studied, it has been possible to analyze the local dynamics, and the results indicate that the same principles established in open-coast and shelf studies are readily transferable to wave-driven sediment transport in estuaries.

[117] Estuarine intertidal flats are in fact excellent natural laboratories that offer a wide range of opportunities for working on a number of fundamental problems in wave-driven sediment transport, including the dynamics of mixed-grain-size beds, the effect of wave fluidization on bed-sediment erodibility, sediment sorting by waves, the effect of waves on sediment flocculation, the effect of fluid acceleration on sediment resuspension, and the effect of groups of high waves on sediment transport. We should be developing these opportunities, seeking “friendly” field sites (accessible, predictable, and not too energetic wave climate and suitable bed sediments) for field experiments that will yield understanding of physical processes that complements advances being made in theory and in laboratory experiments.

[118] An area that is ripe for investigation by exploratory modeling is the interaction between waves, flocculation as it affects particle settling speed, and tidal-flat-scale patterns of sediment transport. Waves contribute to tidal sediment transport by resuspending bed sediments, which adds to any sediment that is suspended by the tidal current. This will always add to the gross tidal transport (loosely defined as the sum of the magnitude of the ebb-tide transport and the magnitude of the flood-tide transport) but will only add significantly to the net tidal transport (loosely defined as the vector sum of the ebb-tide transport and the flood-tide transport) for an optimum range of sediment settling speeds. For settling speeds much smaller than the optimum, wave-resuspended sediment will stay in suspension for many tidal cycles and any extra ebb transport will tend to be canceled by extra flood transport. In contrast, for settling speeds much greater than the optimum, wave-resuspended sediment will be both confined very close to the bed and will settle quickly back to the bed following resuspension, which will reduce the transport of that sediment by the tidal current. *Green and Coco* [2007] took a very small step forward in this area that was motivated by the observation that there was a progressive decoupling of suspended-sediment concentration from the waves on moving from the bottom to the top of a microtidal intertidal flat, which was accompanied by a “hyperconcentration” of suspended sediment on the upper flat. They hypothesized that wave-orbital motions retard sediment settling as sediment is advected up the tidal flat by the flooding tide and that the volume of water available to contain the suspended sediment reduces over the shallow upper flats. A simple exploratory model was developed to test the idea, which revealed how the balance between locally resuspended sediment and suspended sediment that is advected from other source regions changes moving up the flat.

[119] Although there is an understandable emphasis on improving simulation models, which have the aim of making accurate predictions, which in turn will be accomplished by a better understanding of physical processes, we should also be identifying opportunities for building exploratory models. These have proved to be excellent tools for exploring spatial and temporal patterns and poorly understood interactions between processes and between processes and morphology.

SYMBOLS

A	empirical constant in formulation of cohesive-sediment erosion rate
A_1, B_1	empirical constants in formulation of dimensionless wave energy
A_2, B_2	empirical constants in formulation of dimensionless peak wave frequency
A_3, B_3	empirical constants in regression of C on τ_w
A_4	empirical constant in the relationship between C_{ref} and θ'_w
A_b	wave-orbital semiexcursion at the bed
$A_{b,crit}$	wave-orbital semiexcursion at the bed at the initiation sediment motion
B	burst duration
c	wave phase speed
c_g	wave group speed
C	suspended-sediment concentration
C_t	tidal component of the suspended-sediment concentration
C_w	wave component of the suspended-sediment concentration
C_d	drag coefficient
C_{ref}	suspended-sediment reference concentration
D	sediment grainsize
D_{50}	median grainsize of the bed sediment
E	wave energy
E_w	wave erosion work
E_1	component of the cohesive-sediment erosion rate that is due to the buildup of wave-induced pore water pressure
E_2	component of the cohesive-sediment erosion rate that is due to the shear stress exerted by the flow
f	spectral-peak wave frequency
f_w	wave friction factor
f'_w	skin-friction wave friction factor
F	fetch
F_1	function in the formulation of E_1
g	acceleration due to gravity
h	water depth
h_0	water depth at outer end of intertidal flat
h_s	depth at the seaward limit of the zone of wave saturation on an intertidal flat
H	wave height

H_0	wave height at outer end of intertidal flat (water depth = h_0)	$\theta'_{t,wc}$	dimensionless skin friction due to the combined wave current
H_i	incident wave height (impinging on seaward end of intertidal flat)	θ'_w	dimensionless skin friction due to wave
H_s	significant wave height	λ	parameter of the Poisson distribution
k	wave number	ρ	water density
k_b	bed roughness	ρ_s	sediment density
L	wavelength	τ	bed shear stress
m	constant in formulation of dimensionless bed load transport rate	τ_e	critical bed shear stress for erosion of cohesive sediment
M_e	cohesive-sediment erosion rate	τ_c	current-induced bed shear stress
n	constant in formulation of cohesive-sediment erosion rate	τ_w	wave-induced bed shear stress
N	wave action	$\tau_{c,wc}$	current component of $\tau_{t,wc}$
ρ	constant in formulation of dimensionless bed load transport rate	$\tau_{t,wc}$	total combined wave-current bed shear stress
Q_b	bed load sediment transport	$\tau_{w,cross - flat - max}$	cross-flat-maximum wave-induced bed shear stress at any given stage of the tide
RE_w	wave Reynolds number	$\tau_{w,tidal - cycle - max}$	tidal-cycle maximum wave-induced bed shear stress (at any given location on the intertidal flat)
S	sources and sinks in wave-action equation	ν	molecular kinematic viscosity of water
t	time	ϕ_b	direction of bed load transport
T	wave period	Φ_b	dimensionless bed load transport rate
T_{crit}	critical wave period for resuspension of sediment	φ	internal angle of friction
u	easterly component of V	χ	dimensionless fetch
U	tidal current speed	ψ	angle between waves and current
$U_{w,b}$	maximum-over-the-wave-cycle horizontal wave-orbital speed at the bed	ω	wave radian frequency
$U_{w,b,crit}$	critical wave-orbital speed at the bed for initiation of sediment motion	Overbar or $\langle \rangle$	time average
U_{wind}	reference wind speed		
$U_{wind,crit}$	critical wind speed for resuspension of sediment		
V	instantaneous current velocity		
V_t	tidal component of the instantaneous current velocity		
V_w	wave component of the instantaneous current velocity		
v	northerly component of V		
x	horizontal coordinate or distance offshore (positive, from $x = 0$ at the landward end of the intertidal flat)		
X	normalized distance offshore		
y	horizontal coordinate		
z	elevation above the bed		
$z_{\tau_w,max}$	elevation on an intertidal flat corresponding to the maximum in τ_w		
Z_0	seabed hydraulic roughness		
α_1	constant in formulation of E_1		
β	intertidal-flat slope		
δ	dimensionless water depth		
ε_b	bed load efficiency		
ϵ	dimensionless wave energy density		
ζ	dimensionless peak wave frequency		
θ	direction of wave propagation		
θ'_c	dimensionless skin friction due to current		
θ'_{crit}	critical dimensionless skin friction for initiation of sediment motion		

GLOSSARY

Advect transport horizontally by a current.

Asymmetry strictly, nonsymmetry about a vertical axis (see also “skewness”) but commonly used to denote nonsymmetry of any type.

Baroclinic associated with density-induced stratification.

Bathymetry submarine topography.

Bed roughness expressed as a length, a measure of the irregularity of the seabed as it affects dissipation of flow energy by friction. See also “grain roughness” and “hydraulic roughness.”

Bed shear stress tangential force per unit area exerted on the seabed by a flow (either a current, wave, or combined wave-current flow).

Bed load that part of the total sediment transport that is by sediment particles that frequently bounce on or roll along the seabed while being transported by the flow.

Biostabilization a broad term covering a range of biological processes that increase seabed stability and therefore reduce erodibility.

Bioturbation the reworking of sedimentary deposits by living organisms.

Boundary layer the layer of the water column in which current speeds reduce from the free-stream speed (above the boundary layer) to zero at the surface of the seabed.

Cohesive (sediment) a collection of sediment particles that cohere, or stick together, largely due to electrochemical forces.

Drag synonym for “friction.”

Depth-limited breaking the wave breaking that occurs when the water depth reduces to a certain fraction of the wave height (the type of breaking that surfers exploit for fun).

Dewatering loss of water from a bed of sediment.

Dimensionless a quantity that has no physical dimension. For example, a shallow-water wave height may be turned into a dimensionless wave height by dividing by a deepwater wave height.

Ebbing falling of the tide.

Entrainment in the context of this review, drag into or along. See also “reentrainment.”

Event a discrete, as opposed to continuous, occurrence, including storm event, wind event, and resuspension event.

Fetch length of water body over which wind blows to generate waves.

Flocculation the process of aggregating smaller sediment particles together to form larger particles.

Flooding rising of the tide.

Flux synonym for “transport.”

Grain roughness expressed as a length, a measure of the size of individual sediment grains as they affect the generation of skin friction. See also “bed roughness” and “hydraulic roughness.”

Gravitational circulation the circulation of water that is driven by the density difference between saltwater and freshwater.

Halophytic vegetation plants that thrive in saline soil.

Hydraulic roughness expressed as a length, a measure of the loss of energy experienced by water flowing over a seabed as a result of friction.

Hypsometry the distribution of elevations (typically expressed as relative to sea level) of the seabed.

Incident wave height height of waves at the point where they impinge on the outer edge of an intertidal flat.

Interarrival time the time between resuspension events.

Lagrangian a moving frame of reference that follows a water particle, as opposed to a (Eulerian) static frame of reference.

Law of the wall the proposition that the average velocity of a turbulent flow at a given point is proportional to the logarithm of the distance from that point to the solid boundary or the “wall.”

Linear wave theory a simplified (“linearized”) description of surface gravity waves, strictly applicable to waves of zero height, but applied nevertheless to waves of small height and steepness.

Liquefaction the process by which the strength and stiffness of a sediment deposit is reduced as it enters a more liquid state and becomes fluidized.

Locally generated waves waves that are generated more or less in the place where they are encountered. Also called “wind waves.”

Lutocline the interface between clear water on top and a fluid mud beneath.

Macrotidal, mesotidal, microtidal tide ranges in excess of 4 m, 2 to 4 m, and less than 2 m, respectively.

Microphytobenthos the collection of organisms (diatoms, algae, bacteria, and so on) that reside in the surface layer of sediments.

MLLW, MSL, MHHW tide levels mean lower low water, mean sea level, mean higher high water.

Monochromatic a single (wave) period.

Neap tide a tide during the phase of the lunar cycle when tide range is smallest.

Noncohesive (sediment) a collection of sediment particles that do not cohere or stick together.

Parametric expressed in terms of a number of parameters that are derived using certain assumptions.

Percolation in the context herein, water slowly filtering through a porous seabed.

Poisson process a count of the number of events that occur in a certain time interval. The count must have a number of specific properties to be called Poisson.

Pore water pressure the pressure at which pore water is held between grains of sediment.

Pore water water filling the spaces between grains of sediment.

Pseudoplastic a fluid that displays a lower apparent viscosity at some high shear rate.

Quadratic bottom friction friction that is dependent on the square of the velocity, which occurs for a specific range of Reynolds numbers. At lower Reynolds number, which probably occur infrequently in the sea, friction depends linearly on velocity.

Radioisotope dating a method for dating material based on the ratio of a naturally occurring radioactive isotope and its decay product(s).

Reentrainment a term used by some authors to refer specifically to the entrainment of fluid mud.

Reynolds number the ratio of inertial to viscous forces in a flow, indicative of the tendency of a flow to be turbulent.

Rheology the flow of matter, particularly matter that exhibits non-Newtonian behavior, in which viscosity changes with the strain or shear rate.

Ridge and runnel linear sand ridges separated by lower troughs.

Resuspension (of sediment) lifting of sediment particles from the seabed into the water column by fluid forces.

Salinity intrusion movement of saltwater into a body of freshwater.

Salt wedge a wedge-shaped layer (thick at the seaward end; thin at the landward end) of saltwater beneath the seabed and an overlying layer of freshwater.

Scour lag the process by which fine sediments are progressively transported landward under tidal currents (see also “settling lag”). Net landward transport arises when the critical flow speed for resuspension of deposited sediments is greater than the flow speed at which those same sediments become deposited.

Sediment transport the horizontal movement of sediment, either in suspension, in which case the sediment particles are suspended in the water column and they move along with the water, or as bed load, in which case the sediment particles roll, slide, and jump along, in close contact with the seabed.

Settling lag the process by which fine sediments are progressively transported landward under tidal currents (see also “scour lag”). Net landward transport arises because fine sediments take a finite time to reach the bed once the transporting flow falls the speed necessary to keep the sediment in suspension.

Shallow-water equations a simplified form of the equations that describe the conservation of momentum for fluids.

Shoaling increase in wave height that occurs as a wave slows upon moving into shallower water.

Significant wave height the average of the highest one third of the waves in a sea.

Skewness strictly, a nonsymmetry about a horizontal axis. See also “asymmetry.”

Skin friction the component of the bed shear stress that is thought to act on the bed-sediment grains, causing resuspension when the critical bed shear stress for initiation of sediment motion is exceeded.

Slack water the phase of the tide when the tidal-current speed temporarily drops off to zero. Slack water may occur at high tide, low tide, or any time in-between, or it may not occur at all.

Spectral-peak wave frequency (period) the frequency (period) corresponding to the peak in the wave energy spectrum.

Spring tide a tide during the phase of the lunar cycle when tide range is greatest.

Steepness-limited wave breaking the wave breaking that occurs when waves become overly steep, typically producing whitecaps.

Storm surge temporary increase in water level associated with the waves, winds, and low pressures that occur during storms.

Streamline the path traced out by a particle with no mass that is moving with the flow.

Surface gravity waves waves on an air-sea interface, where gravity acts to restore the interface to its equilibrium level following disturbance by (typically) a wind.

Suspended-sediment concentration the mass of sediment suspended in a unit volume of water by the motion of the water.

Time series a sequence of measurements, usually at fixed time intervals, over a certain duration of time.

Viscoelastic having both viscous (able to flow but is resistant to shearing to a large extent) and elastic (resists deformation) properties.

Wave-action (conservation) equation a statement of the conservation of energy by waves.

Wave attenuation reduction in wave height.

Wave dissipation loss of wave energy, typically by friction, resulting in a reduction of wave height.

Wave friction factor by definition, the constant of proportionality in the relationship between wave-induced bed shear stress and the square of the wave-orbital speed. To think of it another way, it is indicative of the fraction of the energy contained by the wave that is dissipated by friction.

Wave-orbital motion circular, elliptical, or back-and-forth current underneath waves.

Wave-orbital speed the speed at which water particles move in an orbital path underneath waves.

Wave-orbital semiexcursion roughly, the diameter of the orbital path traversed by water particles underneath waves.

Wave saturation see “zone of wave saturation.”

Wave-induced shear relative motion between different layers in the water column caused by wave-orbital motions.

Whitecapping see steepness-limited wave breaking.

Wind waves see “locally generated waves”.

Zone of wave saturation the part of the intertidal flat where wave height is proportional to water depth, so that as the water depth decreases, wave height likewise reduces.

[120] **ACKNOWLEDGMENTS.** We are very grateful to Luca Carniello and Giulio Mariotti for their thoughtful and constructive reviews of the manuscript and to the editor-in-chief of *Reviews of Geophysics* for insightful comments and recommendations for making the review more accessible to a wider audience. Any deficiencies in the review, however, remain our responsibility. M.O.G. acknowledges funding from the Ministerio de Educacion, Cultura y Deporte and the Instituto de Hidráulica Ambiental IH Cantabria, University of Cantabria, Spain (SAB2011–0146), the generous support of NIWA, and the Ministry for Business, Innovation and Employment (MBIE C01X1005, Cumulative Effects of Stressors on Aquatic Ecosystems). G.C. acknowledges funding from the AGL programme.

[121] The Editor on this paper was Gregory Okin. He thanks Luca Carniello, Giulio Mariotti, and one anonymous reviewer for their review assistance on this manuscript.

REFERENCES

- Allen, J. R. L. (1984), Sedimentary structures: Their character and physical basis, *Dev. Sedimentol.*, 30, 603.
- Andersen, T. J., and M. Pejrup (2001), Suspended sediment transport on a temperate, microtidal mudflat, the Danish Wadden Sea, *Mar. Geol.*, 173, 69–85.
- Anderson, F. E. (1972), Resuspension of estuarine sediments by small amplitude waves, *J. Sediment. Petrol.*, 42, 602–607.
- Anderson, F. E. (1980), The variation in suspended sediment and water properties in the flood-water front traversing the tidal flat, *Estuaries*, 3, 28–37.
- Anthony, E. J., A. Gardel, N. Gratiot, C. Proisy, M. A. Allison, F. Dolique, and F. Fromard (2010), The Amazon-influenced muddy coast of South America: A review of mud-bank–shoreline interactions, *Earth Sci. Rev.*, 103, 99–121.
- Bailard, J. A. (1981), An energetics total load sediment transport model for a plane sloping beach, *J. Geophys. Res.*, 86, 10,938–10,954.
- Bassoullet, P., P. le Hir, D. Gouleau, and S. Robert (2000), Sediment transport over an intertidal mudflat: Field investigations and estimation of fluxes within the Baie de Marennes-Oléron (France), *Cont. Shelf Res.*, 20(12/13), 1635–1653.

- Booij, N., R. C. Ris, and L. H. Holthuijsen (1999), A third-generation wave model for coastal regions. Part 1: Model description and validation, *J. Geophys. Res.*, *104*(C4), 7649–7666.
- Booth, J. G., R. L. Müller, B. A. McKee, and R. A. Leathers (2000), Wind-induced bottom sediment resuspension in a microtidal coastal environment, *Cont. Shelf Res.*, *20*, 785–806.
- Brampton, A. H. (1992), Engineering significance of British saltmarshes, in *Saltmarshes: Morphodynamics, Conservation, and Engineering Significance*, edited by J. R. L. Allen and K. Pye, Cambridge Univ. Press, Cambridge, UK.
- Bricker, J. D., S. Inagaki, and S. G. Monismith (2005), Bed drag coefficient variability under wind waves in a tidal estuary, *J. Hydraul. Eng.*, *131*(6), 497–508.
- Calliari, L. J., N. S. Speranski, M. Torronteguy, and M. B. Oliveira (2001), The mud banks of Cassino Beach, Southern Brazil: Characteristics, processes and effects, *J. Coastal Res., Spec. Issue*, *34*, 318–325.
- Carling, P. A. (1982), Temporal and spatial variation in intertidal sedimentation rates, *Sedimentology*, *29*(1), 17–23.
- Carniello, L., A. Defina, S. Fagherazzi, and L. D’Alpaos (2005), A combined wind wave–tidal model for the Venice lagoon, Italy, *J. Geophys. Res.*, *110*, F04007, doi:10.1029/2004JF000232.
- Carniello, L., A. D’Alpaos, and A. Defina (2011), Modeling wind waves and tidal flows in shallow micro-tidal basins, *Estuarine Coastal Shelf Sci.*, *92*, 263–276.
- Chen, Q., H. Zhao, K. Hu, and S. L. Douglass (2005), Prediction of wind waves in a shallow estuary, *J. Waterw. Port Coastal Ocean Eng.*, *131*, 137–148.
- Christiansen, C., G. Volund, L. C. Lund-Hansen, and J. Bartholdy (2006), Wind influence on tidal flat sediment dynamics: Field investigations in the Ho Bugt, Danish Wadden Sea, *Mar. Geol.*, *235*, 75–86.
- Christie, M. C., and K. R. Dyer (1998), Measurements of the turbid tidal edge over the Skeffling mudflats, *Geol. Soc. Lond., Spec. Publ.*, *139*, 45–55.
- Christie, M. C., K. R. Dyer, and P. Turner (1999), Sediment flux and bed level measurements from a macro tidal mudflat, *Estuarine Coastal Shelf Sci.*, *49*, 667–688.
- Couperthwaite, J. S., S. B. Mitchell, J. R. West, and D. M. Lawler (1998), Cohesive sediment dynamics on an intertidal bank on the Tidal Trent, UK, *Mar. Pollut. Bull.*, *37*, 144–154.
- D’Alpaos, A., L. Carniello, and A. Rinaldo (2013), Statistical mechanics of wind wave-induced erosion in shallow tidal basins: Inferences from the Venice Lagoon, *Geophys. Res. Lett.*, *40*, 3402–3407, doi:10.1002/grl.50666.
- de Haas, H., and D. Eisma (1993), Suspended-sediment transport in the Dollard estuary, *Neth. J. Sea Res.*, *31*(1), 37–42.
- de Jonge, V. N., and J. E. E. van Beusekom (1992), Contribution of resuspended microphytobenthos to total phytoplankton in the Ems estuary and its possible role for grazers, *Neth. J. Sea Res.*, *30*, 91–105.
- de Jonge, V. N., and J. E. E. van Beusekom (1995), Wind- and tide-induced resuspension of sediment and microphytobenthos from tidal flats in the Ems estuary, *Limnol. Oceanogr.*, *40*(4), 788–778.
- de Swart, H. E., and J. T. F. Zimmerman (2009), Morphodynamics of tidal inlet systems, *Annu. Rev. Fluid Mech.*, *41*, 203–229, doi:10.1146/annurev.fluid.010908.165159.
- Defina, A., L. Carniello, S. Fagherazzi, and L. D’Alpaos (2007), Self-organization of shallow basins in tidal flats and salt marshes, *J. Geophys. Res.*, *112*, F03001, doi:10.1029/2006JF000550.
- Demers, S., J.-C. Therriault, E. Bourget, and A. Bah (1987), Resuspension in the shallow sublittoral zone of a macrotidal estuarine environment: Wind influence, *Limnol. Oceanogr.*, *32*, 327–339.
- Dolphin, T. J., and M. O. Green (2009), Patterns of wave-orbital speed and skin friction under estuarine (fetch-limited) waves, *J. Coastal Res., Spec. Issue*, *56*, 178–182.
- Dolphin, T. J., T. M. Hume, and K. E. Parnell (1995), Oceanographic processes and sediment mixing on a sand flat in an enclosed sea, Manukau Harbour, New Zealand, *Mar. Geol.*, *128*, 169–181.
- Dronkers, J. (1986), Tidal asymmetry and estuarine morphology, *Neth. J. Sea Res.*, *20*(2), 117–131.
- Dyer, K. R., M. C. Christie, N. Feates, M. J. Fennessy, M. Pejrup, and W. van der Lee (2000), An investigation into processes influencing the morphodynamics of an intertidal mudflat, the Dollard Estuary, the Netherlands: I. Hydrodynamics and suspended sediment, *Cont. Shelf Res.*, *50*(5), 607–625.
- Ellis, J. E., V. J. Cummings, J. E. Hewitt, S. F. Thrush, and A. Norkko (2002), Determining effects of suspended sediment on condition of a suspension feeding bivalve (*Atrina zelandica*): Results of a survey, a laboratory experiment and a field transplant experiment, *J. Exp. Mar. Biol. Ecol.*, *267*(2), 147–174.
- Etamad-Shahidi, A., M. Kazeminezhad, and J. Mousavi (2009), On the prediction of wave parameters using simplified methods, *J. Coastal Res.*, *SI56*, 505–509.
- Fagherazzi, S., and P. L. Wiberg (2009), Importance of wind conditions, fetch, and water levels on wave-generated shear stresses in shallow intertidal basins, *J. Geophys. Res.*, *114*, F03022, doi:10.1029/2008JF001139.
- Fagherazzi, S., L. Carniello, L. D’Alpaos, and A. Defina (2006), Critical bifurcation of shallow microtidal landforms in tidal flats and salt marshes, *Proc. Natl. Acad. Sci. U. S. A.*, *103*, 8337–8341.
- Fagherazzi, S., C. Palermo, M. C. Rulli, L. Carniello, and A. Defina (2007), Wind waves in shallow microtidal basins and the dynamic equilibrium of tidal flats, *J. Geophys. Res.*, *112*, F02024, doi:10.1029/2006JF000572.
- Fagherazzi, S., et al. (2012), Numerical models of salt marsh evolution: Ecological, geomorphic, and climatic factors, *Rev. Geophys.*, *50*, RG1002, doi:10.1029/2011RG000359.
- Ferrarin, C., G. Umgiesser, A. Cucco, T. Hsu, A. Roland, and C. L. Amos (2008), Development and validation of a finite element morphological model for shallow water basins, *Coastal Eng.*, *55*, 716–731.
- Foda, M. A., and H.-C. Huang (2001), A fluidization model for cross-shore sediment transport by water waves, *Waves 2001 Conference*, American Society of Civil Engineers, September, 2001, San Francisco, Calif.
- Francalanci, S., M. Bondoni, M. Rinaldi, and L. Solari (2013), Ecomorphodynamic evolution of salt marshes: Experimental observations of bank retreat processes, *Geomorphology*, *195*, 53–65, doi:10.1016/j.geomorph.2013.04.026.
- Friedrichs, C. L. (2011), Tidal flat morphodynamics: A synthesis, in *Treatise on Estuarine and Coastal Science*, vol. 3, Estuarine and Coastal Geology and Geomorphology, edited by J. D. Hansom and B. W. Fleming, pp. 137–170, Elsevier, Amsterdam, Netherlands.
- Friedrichs, C. T., and D. G. Aubrey (1996), Uniform bottom shear stress and equilibrium hypsometry of intertidal flats, in *Mixing in Estuaries and Coastal Seas*, Coastal Estuarine Studies, vol. 50, edited by C. Pattiaratchi, pp. 405–429, AGU, Washington, D.C., doi:10.1029/CE050p0405.
- Friedrichs, C. T., and J. E. Perry (2001), Tidal salt marsh morphodynamics: A synthesis, *J. Coastal Res.*, *SI*(27), 7–37.
- Gabrielson, J. O., and R. J. Lukatelich (1985), Wind-related resuspension of sediments in the Peel-Harvey Estuarine System, *Estuarine Coastal Shelf Sci.*, *20*(2), 135–145.
- Gouleau, D., J. M. Jouanneau, O. Weber, and P. G. Sauriau (2000), Short- and long-term sedimentation on Montportail–Brouage intertidal mudflat, Marennes–Oleron Bay (France), *Cont. Shelf Res.*, *20*(12/13), 1513–1530.
- Graf, W. H. (1971), *Hydraulics of Sediment Transport*, pp. 513, McGraw-Hill, New York.
- Green, M. O. (2011), Dynamics of very small waves and associated sediment resuspension on an estuarine intertidal flat, *Estuarine Coastal Shelf Sci.*, *93*(4), 449–459.
- Green, M. O., and K. P. Black (1999), Suspended-sediment reference concentration under waves: Field observations and critical analysis of two predictive models, *Coastal Eng.*, *38*, 115–141.
- Green, M. O., and G. Coco (2007), Sediment transport on an estuarine intertidal flat: Measurements and conceptual model of waves, rainfall and exchanges with a tidal creek, *Estuarine Coastal Shelf Sci.*, *72*, 553–569.

- Green, M. O., and N. J. Hancock (2012), Sediment transport through a tidal creek, *Estuarine Coastal Shelf Sci.*, 109, 116–132.
- Green, M. O., and I. T. MacDonald (2001), Processes driving estuary infilling by marine sands on an embayed coast, *Mar. Geol.*, 178(1/4), 11–37.
- Green, M. O., K. P. Black, and C. L. Amos (1997), Control of estuarine sediment dynamics by interactions between currents and waves at several scales, *Mar. Geol.*, 144, 97–116.
- Green, M. O., R. G. Bell, T. J. Dolphin, and A. Swales (2000), Silt and sand transport in a deep tidal channel of a large estuary (Manukau Harbour, New Zealand), *Mar. Geol.*, 163, 217–240.
- Hasselmann, K. et al. (1973), Measurements of wind-wave growth and swell decay during the Joint North Sea Wave Project (JONSWAP), *Dtsch. Hydrogr. Zeit. Suppl.*, 12(A8), 1–95.
- Hoekstra, P., P. Bell, P. van Santen, N. Roode, F. Levoy, and R. Whitehouse (2004), Bedform migration and bedload transport on an intertidal shoal, *Cont. Shelf Res.*, 24, 1249–1269.
- Jackson, N. L., K. F. Nordstrom, I. Eliot, and G. Masselink (2002), ‘Low energy’ marine and estuarine beaches: A review, *Geomorphology*, 48, 147–162.
- Janssen-Stelder, B. (2000), The effect of different hydrodynamic conditions on the morphodynamics of a tidal mudflat in the Dutch Wadden Sea, *Cont. Shelf Res.*, 20(12/13), 1461–1478.
- Kim, B. O. (2003), Tidal modulation of storm waves on a macrotidal flat in the Yellow Sea, *Estuarine Coastal Shelf Sci.*, 57, 411–420.
- Kineke, G. C., R. W. Sternberg, J. H. Trowbridge, and W. R. Geyer (1996), Fluid-mud processes on the Amazon continental shelf, *Cont. Shelf Res.*, 16(5/6), 667–696.
- Kirby, R. (1986), Suspended fine cohesive sediment in the Severn Estuary and Inner Bristol Channel, UK. *Report No. ETSU-STP-4042 to the UK Atomic Energy Authority*, Ravensrodd Consultants Ltd, Taunton, U.K., 243.
- Kirby, R., and W. R. Parker (1983), Distribution and behaviour of fine sediment in the Severn Estuary and Inner Bristol Channel, UK, *Can. J. Fish. Aquat. Sci.*, 40(Suppl. 1), 83–95.
- Kirby, R., R. J. Bleakley, S. T. C. Weatherup, P. J. Raven, and N. D. Donaldson (1993), Effect of episodic events on tidal mud flat stability, Ardmillan Bay, Strangford Lough, Northern Ireland, in *Nearshore and Estuarine Cohesive Sediment Transport*, edited by A. J. Mehta, pp. 378–392, AGU, Washington, D.C.
- Kitheka, J. U., M. Obiero, and P. Nthenge (2005), River discharge, sediment transport and exchange in the Tana Estuary, Kenya, *Estuarine Coastal Shelf Sci.*, 63, 455–468.
- Komar, P. D., and M. C. Miller (1973), The threshold of sediment movement under oscillatory water waves, *J. Sediment. Petrol.*, 43(4), 1101–1110.
- Komar, P. D., and M. C. Miller (1975), On the comparison between the threshold of sediment motion under waves and unidirectional currents with a discussion of the practical evaluation of the threshold, *J. Sediment. Petrol.*, 45, 362–367.
- Kuo, Y.-Y., and Y.-F. Chiu (1994), Transfer function between the wave height and wave pressure for progressive waves, *Coastal Eng.*, 23, 81–93.
- Lambrechts, J., C. Humphrey, L. McKinna, O. Gorge, K. E. Fabricius, A. J. Mehta, S. Lewis, and E. Wolanski (2010), Importance of wave-induced bed liquefaction in the fine sediment budget of Cleveland Bay, Great Barrier Reef, *Estuarine Coastal Shelf Sci.*, 89(2), 154–162.
- Lawson, S. E., P. L. Wiberg, K. J. McGlathery, and D. C. Fugate (2007), Wind-driven sediment suspension controls light availability in a shallow coastal lagoon, *Estuaries Coasts*, 30(1), 102–112.
- le Hir, P., W. Roberts, O. Cazaillet, M. Christie, P. Bassoullet, and C. Bacher (2000), Characterization of intertidal flat hydrodynamics, *Cont. Shelf Res.*, 20(12/13), 1433–1459.
- Lettmann, K. A., J. Wolff, and T. H. Badewien (2009), Modeling the impact of wind and waves on suspended particulate matter fluxes in the East Frisian Wadden Sea (Southern North Sea), *Ocean Dyn.*, doi:10.1007/s10236-009-0194-5.
- Lewis, R. R., M. J. Durako, M. D. Moffler, and Phillips (1985), Seagrass meadows of Tampa Bay—A review, in *Proceedings of the Tampa Bay Area Scientific Information Systems*, edited by S. F. Treat et al., pp. 210–216, Bellwether Press, Minneapolis.
- Li, J., and C. Zhang (1998), Sediment resuspension and implications for turbidity maximum in the Changjiang Estuary, *Mar. Geol.*, 148(3/4), 117–124.
- Li, Y., and A. J. Mehta (1997), Mud fluidization by water waves, in *Cohesive Sediments*, edited by N. Burt, R. Parker and J. Watts, pp. 341–351, Wiley, New York.
- Maa, P.-Y., and A. Mehta (1987), Mud erosion by waves: A laboratory study, *Cont. Shelf Res.*, 7, 1269–1284.
- Malvarez, G. C., J. A. G. Cooper, and D. W. T. Jackson (2001), Relationships between wave-induced currents and sediment grain size on a sandy tidal-flat, *J. Sediment. Res.*, 71(5), 705–712.
- Marani, M., A. D’Alpaos, S. Lanzoni, L. Carniello, and A. Rinaldo (2010), The importance of being coupled: Stable states and catastrophic shifts in tidal biomorphodynamics, *J. Geophys. Res.*, 115, F04004, doi:10.1029/2009JF001600.
- Marani, M., A. D’Alpaos, S. Lanzoni, and M. Santalucia (2011), Understanding and predicting wave erosion of marsh edges, *Geophys. Res. Lett.*, 38, L21401, doi:10.1029/2011GL048995.
- Mariotti, G., and S. Fagherazzi (2011), Asymmetric fluxes of water and sediments in a mesotidal mudflat channel, *Cont. Shelf Res.*, 31, 23–36.
- Mariotti, G., and S. Fagherazzi (2013a), Critical width of tidal flats triggers marsh collapse in the absence of sea-level rise, *Proc. Natl. Acad. Sci. U. S. A.*, 110(14), 5353–5356.
- Mariotti, G., and S. Fagherazzi (2013b), Wind waves on a mudflat: The influence of fetch and depth on bed shear stresses, *Cont. Shelf Res.*, 60S, S99–S110.
- Mariotti, G., and S. Fagherazzi (2013c), A two-point dynamic model for the coupled evolution of channels and tidal flats, *J. Geophys. Res. Earth Surf.*, 118, 1–13, doi:10.1002/jgrf.20070.
- Mathew, J., M. Baba, and N. P. Kurian (1995), Mudbanks of the southwest coast of India. I. Wave characteristics, *J. Coastal Res.*, 11(1), 168–178.
- McAnally, W. H., C. Friedrichs, D. Hamilton, E. Hayter, P. Shresthar, H. Rodriguez, A. Sheremet, and A. Teeter (2007), Management of fluid mud in estuaries, bays, and lakes. 1. Present state of understanding on character and behavior, *J. Hydraul. Eng.*, 133(1), 9–22.
- Mehta, A. J. (1991), Understanding fluid mud in a dynamic environment, *Geo Mar. Lett.*, 11, 113–118.
- Mehta, A. J. (1996), Interaction between fluid mud and water waves, in *Environmental Hydraulics*, edited by V. P. Singh and W. H. Hager, chap. 5, 153–187, Kluwer, Dordrecht, Netherlands.
- Mehta, A. J., and R. Srinivas (1993), Observations on the entrainment of fluid mud by shear flow, in *Nearshore and Estuarine Cohesive Sediment Transport*, vol. 42, Coastal and Estuarine Studies, edited by A. J. Mehta, pp. 224–246, AGU, Washington, D. C.
- Mehta, A. J., E. J. Hayter, W. R. Parker, R. B. Krone, and A. M. Teeter (1989), Cohesive sediment transport. I: Process description, *J. Hydraul. Eng.*, 115, 1076–1093.
- Mitchell, S. B., J. S. Couperthwaite, J. R. West, and D. M. Lawler (2003), Measuring sediment exchange rates on an intertidal bank at Blacktoft, Humber Estuary, UK, *Sci. Total Environ.*, 314–316, 535–549.
- Mitchener, H., and H. Torfs (1996), Erosion of mud/sand mixtures, *Coastal Eng.*, 29, 1–25.
- Moller, I., T. Spencer, J. R. French, D. J. Leggett, and M. Dixon (1999), Wave transformation over salt marshes: A field and numerical modelling study from North Norfolk, England, *Estuarine Coastal Shelf Sci.*, 49, 411–426.
- Moore, K. A., and R. L. Wetzel (2000), Seasonal variations in eelgrass (*Zostera marina* L.) responses to nutrient enrichment and reduced light availability in experimental ecosystems, *J. Exp. Mar. Biol. Ecol.*, 244, 1–28.

- Murray, A. B. (2003), Contrasting the goals, strategies, and predictions associated with simplified models and detailed simulations, *Geophys. Monogr. Ser.*, 135, 151–165.
- Nichols, M. M. (1985), Fluid mud accumulation processes in estuaries, *Geo Mar. Lett.*, 4, 171–176.
- Nielsen, P. (1992), *Coastal Bottom Boundary Layers and Sediment Transport*, pp. 324, World Scientific, Singapore.
- Nordstrom, K. F., and N. L. Jackson (2012), Physical processes and landforms on beaches in short fetch environments in estuaries, small lakes and reservoirs: A review, *Earth Sci. Rev.*, 111, 232–247.
- Norkko, A., S. F. Thrush, J. E. Hewitt, V. J. Cummings, J. Norkko, J. I. Ellis, G. A. Funnell, D. Schultz, and I. T. MacDonald (2002), Smothering of estuarine sandflats by terrigenous clay: The role of wind-wave disturbance and bioturbation in site-dependent macrofaunal recovery, *Mar. Ecol. Prog. Ser.*, 234, 23–41.
- Nowacki, D. J., and A. S. Ogston (2012), Water and sediment transport of channel-flat systems in a mesotidal mudflat: Willapa Bay, Washington, *Cont. Shelf Res.*, doi:10.1016/j.csr.2012.07.019.
- Pejrup, M. (1988), Suspended sediment transport across a tidal flat, *Mar. Geol.*, 82, 187–198.
- Postma, H. (1961), Transport and accumulation of suspended matter in the Dutch Wadden Sea, *Neth. J. Sea Res.*, 1, 148–190.
- Pritchard, D. (2005), Suspended sediment transport along an idealised tidal embayment: Settling lag, residual transport and the interpretation of tidal signals, *Ocean Dyn.*, 55, 124–136.
- Quaresma, V. S., A. C. Bastos, and C. L. Amos (2007), Sedimentary processes over an intertidal flat: A field investigation at Hythe flats, Southampton Water (UK), *Mar. Geol.*, 241(1/4), 117–136.
- Ralston, D. K., and M. T. Stacey (2007), Tidal and meteorological forcing of sediment transport in tributary mudflat channels, *Cont. Shelf Res.*, 27(10–11), 1510–1527.
- Ribberink, J. S. (1998), Bed load transport for steady flows and unsteady oscillatory flows, *Coastal Eng.*, 34, 59–82.
- Ridderinkhof, H. (1998), On the sensitivity of the large scale transport and distribution of fine-grained sediments in a tidal basin to the formulation of the erosion-sedimentation cycle, in *Physics of Estuaries and Coastal Seas*, edited by J. Dronkers and M. Sheffers, pp. 145–153, Balkema, Rotterdam, Netherlands.
- Ridderinkhof, H., R. van der Ham, and W. van der Lee (2000), Temporal variations in concentration and transport of suspended sediments in a channel-flat system in the Ems-Dollard estuary, *Cont. Shelf Res.*, 20(12/13), 1479–1493.
- Roberts, W., P. le Hir, and R. J. S. Whitehouse (2000), Investigations using simple mathematical models of the effect of tidal currents and waves on the profile shape of intertidal mudflats, *Cont. Shelf Res.*, 20, 1079–1097.
- Rodriguez, H. N., and A. J. Mehta (1998), Considerations on wave-induced fluid mud streaming at open coasts, in *Sedimentary Processes in the Intertidal Zone*, *Geological Soc.*, vol. 139, edited by K. S. Black, D. M. Paterson, and A. Cramp, pp., 177–186 Special Publications, London, U.K.
- Rodriguez, H. N., and A. J. Mehta (2000), Longshore transport of fine-grained sediment, *Cont. Shelf Res.*, 20, 1419–1432.
- Ross, M. A., and A. J. Mehta (1989), On the mechanics of lutoclines and fluid mud, *J. Coastal Res.*, 5, 51–61.
- Ruhl, C. A., D. H. Schoellhamer, R. P. Stumpf, and C. L. Lindsay (2001), Combined use of remote sensing and continuous monitoring to analyze the variability of suspended-sediment concentrations in San Francisco Bay, California, *Estuarine Coastal Shelf Sci.*, 53, 801–812.
- Ryan, N. M., and J. A. G. Cooper (1998), Spatial variability of tidal flats in response to wave exposure: Examples from Strangford Lough, Co. Down, Northern Ireland, *Geol. Soc. Spec. Publ.*, 139, 221–230.
- Sanford, L. P. (1994), Wave-forced resuspension of upper Chesapeake Bay muds, *Estuaries*, 17(1B), 148–165.
- Scarlato, P. D., and A. J. Mehta (1990), Some observations on erosion and entrainment of estuarine fluid muds, in *Coastal and Estuarine Studies 38, Residual Currents and Long-Term Transport*, edited by R. T. Cheng, pp. 321–332, Springer-Verlag, New York.
- Schoellhamer, D. H. (1995), Sediment resuspension mechanisms in Old Tampa Bay, Florida, *Estuarine Coastal Shelf Sci.*, 40, 603–620.
- Sheremet, A., S. Jaramillo, S.-F. Su, M. A. Allison, and Holland, K. T. (2011), Wave-mud interaction over the muddy Atchafalaya subaqueous clinoform, Louisiana, United States: Wave processes, *J. Geophys. Res.*, 116, C06005, doi:10.1029/2010JC006644.
- Shi, Z., and J. Y. Chen (1996), Morphodynamics and sediment dynamics on intertidal mudflats in China (1961–1994), *Cont. Shelf Res.*, 16, 1909–1926.
- Shi, N. C., and L. H. Larsen (1984), Reverse sediment transport induced by amplitude-modulated waves, *Mar. Geol.*, 54, 181–200.
- Shi, Z., L. F. Ren, S. Y. Zhang, and J. Y. Chen (1997), Acoustic imaging of cohesive sediment resuspension and re-entrainment in the Changjiang Estuary, East China Sea, *Geo Mar. Lett.*, 17, 162–168.
- Shi, J. Z., M. E. Luther, and S. Meyers (2006), Modelling of wind wave-induced bottom processes during the slack water periods in Tampa Bay, Florida, *Int. J. Numer. Methods Fluids*, 52, 1277–1292.
- Smith, J. D., and S. R. McLean (1977), Spatially averaged flow over a wavy surface, *J. Geophys. Res.*, 82(12), 1735–1746.
- Smith, M. J., C. L. Stevens, R. M. Gorman, J. A. McGregor, and C. G. Neilson (2001), Wind-wave development across a large shallow intertidal estuary: A case study of Manukau Harbour, New Zealand, *N.Z. J. Mar. Freshwater Res.*, 35(5), 985–1000.
- Soulsby, R. L. (1995), Bed shear stress due to combined waves and currents, in *Advances in Coastal Morphodynamics*, edited by M. J. F. Stive et al., pp. 4:20–4:23, Delft Hydraulics, Delft, The Netherlands.
- Soulsby, R. L. (1997), *Dynamics of Marine Sands*, pp. 429, Thomas Telford, London, U.K.
- Soulsby, R. L., L. Hamm, G. Klopmann, D. Myrhaug, R. R. Simons, and G. P. Thomas (1993), Wave-current interaction within and outside the bottom boundary layer, *Coastal Eng.*, 21, 41–69.
- Spearman, J. (2011), The development of a tool for examining the morphological evolution of managed realignment sites, *Cont. Shelf Res.*, 31, 199–210.
- Swart, D. H. (1974), Offshore sediment transport and equilibrium beach profiles. *Ph.D. dissertation*, Dep. of Civ. Eng., Delft Univ. of Technol., Delft, Netherlands.
- Talke, S. A., and M. T. Stacey (2003), The influence of oceanic swell on flows over an estuarine intertidal mudflat in San Francisco Bay, *Estuarine Coastal Shelf Sci.*, 58(3), 541–554.
- Tambroni, N., and G. Seminara (2012), A one-dimensional eco-geomorphic model of marsh response to sea level rise: Wind effects, dynamics of the marsh border and equilibrium, *J. Geophys. Res.*, 117, F03026, doi:10.1029/2012JF002363.
- Townend, I., C. Fletcher, M. Knappen, and K. Rossington (2011), A review of salt marsh dynamics, *Water Environ. J.*, 25, 477–488.
- Tsai, C.-H., M.-C. Huang, F.-J. Young, Y.-C. Lin, and H.-W. Li (2005), On the recovery of surface wave by pressure transfer function, *Ocean Eng.*, 32, 1247–1259.
- Turner, S. J., J. E. Hewitt, M. R. Wilkinson, D. J. Morrissey, S. F. Thrush, V. J. Cummings, and G. Funnell (1999), Seagrass patches and landscapes: The influence of wind-wave dynamics and hierarchical arrangements of spatial structure on macrofaunal seagrass communities, *Estuaries Coasts*, 22(4), 1016–1032.
- U.S. Army Coastal Engineering Research Center (1984), *Shore Protection Manual*, vol. 1, 4th ed., pp. 603, U.S. Army Coastal Engineering Center, Fort Belvoir, Va.
- Umgiesser, G., M. Sclavo, S. Carniel, and A. Bergamasco (2004), Exploring the bottom stress variability in the Venice Lagoon, *J. Mar. Syst.*, 51, 161–178.

- Uncles, R. J., and J. A. Stephens (2000), Observations of currents, salinity, turbidity and intertidal mudflat characteristics and properties in the Tavy Estuary, UK, *Cont. Shelf Res.*, 20, 1531–1549.
- Uncles, R. J., and J. A. Stephens (2010), Turbidity and sediment transport in a muddy sub-estuary, *Estuarine Coastal Shelf Sci.*, 87(2), 213–214.
- Uncles, R. J., J. A. Stephens, and D. J. Law (2006), Turbidity maximum in the macrotidal, highly turbid Humber Estuary, UK: Flocs, fluid mud, stationary suspensions and tidal bores, *Estuarine Coastal Shelf Sci.*, 67, 30–52.
- van Straaten, L. M. J. U., and P. H. Kuenen (1957), Accumulation of fine-grained sediments in the Dutch Wadden Sea, *Geol. Mijnbouw*, 19e, 329–354.
- van Rijn, L. C. (1990), *Principles of Fluid Flow and Surface Waves in Rivers, Estuaries, Seas and Oceans*, pp. 335, Aqua Publications, Oldemarkt.
- van Ledden, M., W. G. M. van Kesteren, and J. C. Winterwerp (2004), A conceptual framework for the erosion behaviour of sand–mud mixtures, *Cont. Shelf Res.*, 24(1), 1–11.
- van der Lee, W. T. B. (1998), The impact of fluid shear and the suspended sediment concentration on the mud floc size variation in the Dollard estuary, The Netherlands, in *Sedimentary Processes in the Intertidal Zone*, vol. 139, edited by K. S. Black, D. M. Paterson and A. Cramp, pp. 187–198, Geological Society, Special Publications, London, U.K.
- Verney, R., J. Deloffre, J.-C. Brun-Cottan, and R. Lafite (2007), The effect of wave-induced turbulence on intertidal mudflats: Impact of boat traffic and wind, *Cont. Shelf Res.*, 27(5), 594–612.
- Verspecht, F., and C. Pattiaratchi (2010), On the significance of wind event frequency for particulate resuspension in coastal waters, *Cont. Shelf Res.*, 30, 1971–1982.
- Wang, Y., D. Zhu, and X. Wu (2002), Chapter Thirteen Tidal flats and associated muddy coast of China, *Proceedings in Marine Science*, 4, 319–345.
- Wang, C., and S. Temmerman (2013), Does biogeomorphic feedback lead to abrupt shifts between alternative landscape states?: An empirical study on intertidal flats and marshes, *J. Geophys. Res. Earth Surf.*, 118, 229–240, doi:10.1029/2012JF002474.
- Weir, D. J., and J. McManus (1987), The role of wind in generating turbidity maxima in the Tay Estuary, *Cont. Shelf Res.*, 2(11/12), 1315–1318.
- Wells, J. T., and G. P. Kemp (1986), Interaction of surface waves and cohesive sediments: Field observations and geologic significance, in *Estuarine Cohesive Sediment Dynamics*, Lecture Notes on Coastal and Estuarine Studies N314, edited by A. J. Mehta, pp. 43–65, Springer, Berlin, Germany.
- Widdows, J., M. D. Brinsley, P. N. Salkeld, and C. H. Lucas (2000), Influence of biota on spatial and temporal variation in sediment erodability and material flux on a tidal flat (Westerschelde, The Netherlands), *Mar. Ecol. Prog. Ser.*, 194, 23–378.
- Williamson, R. B., L. F. van Dam, R. G. Bell, and M. O. Green (1996), Heavy metal and suspended sediment fluxes from a contaminated, intertidal inlet (Manukau Harbour, New Zealand), *Mar. Pollut. Bull.*, 32(11), 812–822.
- Winterwerp, J. C. (1999), On the dynamics of high-concentrated mud suspensions. PhD thesis, Delft University of Technology, Delft, The Netherlands, 171.
- Winterwerp, J. C. (2002), On the flocculation and settling velocity of estuarine mud, *Cont. Shelf Res.*, 22, 1339–1360.
- Wolanski, E., and S. Spagnol (2003), Dynamics of the turbidity maximum in King Sound, tropical Western Australia, *Estuarine Coastal Shelf Sci.*, 56(5/6), 877–890.
- Wolanski, E., J. Chappell, P. Ridd, and R. Vertessy (1988), Fluidization of mud in estuaries, *J. Geophys. Res.*, 93(C3), 2351–2361.
- Wolanski, E., B. King, and D. Galloway (1995), Dynamics of the turbidity maximum in the Fly River Estuary, Papua New Guinea, *Estuarine Coastal Shelf Sci.*, 40, 321–337.
- Wright, L. D., J. D. Boon, J. P. Xu, and S. C. Kim (1992), The bottom boundary layer of the bay stem plains environment of lower Chesapeake Bay, *Estuarine Coastal Shelf Sci.*, 35(1), 17–36.
- Yang, S.-L., C. T. Friedrichs, Z. Shi, P.-X. Ding, J. Zhu, and Q.-Y. Zhao (2003), Morphological response of tidal marshes, flats and channels of the outer Yangtze River mouth to a major storm, *Estuaries*, 26(6), 1416–1425.
- Young, I. R., and L. A. Verhagen (1996a), The growth of fetch limited waves in water of finite depth. 1. Total energy and peak frequency, *Coastal Eng.*, 29(1–2), 47–78, doi:10.1016/S0378-3839(96)00006-3.
- Young, I. R., and L. A. Verhagen (1996b), The growth of fetch limited waves in water of finite depth. 2. Spectral evolution, *Coastal Eng.*, 29(1–2), 79–99, doi:10.1016/S0378-3839(96)00007-5.